

Cannabinoid receptor CB₂ drives HER2 pro-oncogenic signaling in breast cancer

Eduardo Pérez-Gómez, Clara Andradas, María M. Caffarel, Sandra Blasco-Benito, Elena García-Taboada, María Villa-Morales, Estefanía Moreno, Sigrid Hamann, Ester Martín-Villar, Juana M. Flores, Antonia Wengers, Ibrahim Alkatout, Wolfram Klapper, Christoph Röcken, Peter Bronsert, Elmar Stickeler, Annette Staebler, Maret Bauer, Norbert Arnold, Joaquim Soriano, Manuel Pérez-Martínez, Diego Megías, Gema Moreno-Bueno, Silvia Ortega-Gutiérrez, Marta Artola, Henar Vázquez-Villa, Miguel Quintanilla, José Fernández-Piqueras, Enric I. Canela, Peter J. McCormick, Manuel Guzmán and Cristina Sánchez

Correspondence to: Cristina Sánchez, Eduardo Pérez-Gómez, Dept. Biochemistry and Molecular Biology I, School of Biology, Complutense University, Madrid 28040 Spain.

Phone: (+34) 913944668. Fax: (+34) 913944672. E-mails:

cristina.sanchez@quim.ucm.es, eperez@bbml.ucm.es

Background Pharmacological activation of cannabinoid receptors elicits antitumoral responses in different models of cancer. However, the biological role of these receptors in tumor physio-pathology is still unknown.

Methods We analyzed CB₂ cannabinoid receptor protein expression in two series of 166 and 483 breast tumor samples operated in the University Hospitals of Kiel, Tübingen and Freiburg between 1997 and 2010. CB₂ mRNA expression was also analyzed in previously published DNA microarray datasets. The role of CB₂ in oncogenesis was studied by generating a mouse line that expresses the HER2 rat ortholog (neu) and lacks CB₂, and by a variety of biochemical and cell biology approaches in human breast cancer cells in culture and *in vivo*, upon modulation of CB₂ expression by si/shRNAs and overexpression plasmids. CB₂-HER2 molecular interaction was studied by co-localization, co-immunoprecipitation and proximity ligation assays.

Results We show an association between elevated CB₂ expression in HER2+ breast tumors and poor patient prognosis. We also demonstrate that genetic inactivation of CB₂ impairs tumor generation and progression in MMTV-neu mice. Moreover, we show that HER2 upregulates CB₂ expression by activating the transcription factor ELK1 via the ERK cascade, and that an increased CB₂ expression activates the HER2 pro-oncogenic signaling machinery at the level of the tyrosine kinase c-SRC. Finally, HER2 and CB₂ form heteromers in cancer cells.

Conclusions Our findings reveal an unprecedented role of CB₂ as a pivotal regulator of HER2 pro-oncogenic signaling in breast cancer, and suggest that CB₂ may be a biomarker with prognostic value in these tumors.

The classical and the most recent molecular classification of breast cancer recognize a specific entity characterized by the overexpression of the tyrosine kinase receptor (TKR) HER2 (1-4). Activation of TKRs turns on key signaling pathways involved in cell proliferation, development, differentiation, and angiogenesis, among other processes (5). HER2 gene amplification/protein overexpression is detected in 20-30% of primary breast cancers, and is a predictor of poor prognosis and deficient response to chemotherapy (6).

The endocannabinoid system (ECS) is a cell-communication system that participates in the control of different physiological functions such as pain perception, motor behavior and food intake, just to mention a few (7, 8). It consists of two cannabinoid-specific G protein-coupled receptors (GPCRs), CB₁ and CB₂, their endogenous ligands, and the enzymes that produce and metabolize these ligands (7, 8). A large number of studies demonstrates that the pharmacological activation of the ECS by different strategies (e.g. activation of cannabinoid receptors, inhibition of endocannabinoid degradation) leads to antitumoral responses (7-11). In addition, it has been shown that the ECS is deregulated in a variety of cancers (7, 12, 13). Although strong evidence points to the cannabinoid receptor CB₂ as a drug target for antitumoral therapy in several types of cancer (11, 14), there is no information on its role in tumor generation and progression. Here we show an unprecedented pro-oncogenic role of the cannabinoid receptor CB₂ in HER2+ breast cancer, and unveil that this GPCR is a pivotal regulator of HER2 signaling.

Methods

Tissue microarrays

PFA-fixed and paraffin-embedded blocks of tumor tissue from cases operated in the University Hospitals of Kiel, Tübingen or Freiburg between 1997 and 2010 were used for tissue microarray (TMA) construction by punching two 1-mm spots of each patient's sample. This resulted in two series of 166 and 483 tumor samples. Complete histopathological information was available for all the patients. In addition, for the 483-sample series (TMA #2), date and cause of death as well as date of local and/or distant relapse were also available.

Immunohistochemical analysis

Tissue sections were subjected to a heat-induced antigen retrieval step prior to exposure to an anti-CB₂ receptor or an anti-ERBB2 primary antibody (Supplemental Table 1).

Immunodetection was performed using the Envision method with DAB as the chromogen. For CB₂ expression, cases were scored as 0 (no staining), 1 (weak staining), 2 (moderate staining) or 3 (high staining). ERBB2-staining was scored according to HercepTest manufacturer's guidelines.

Generation of MMTV-neu:CB₂^{-/-} mice and sample collection

All procedures involving animals were performed with the approval of the Complutense University Animal Experimentation Committee according to the EU official regulations. Generation of the congenic strain MMTV-neu:CB₂^{-/-} was accomplished by mating MMTV-neu mice with CB₂^{-/-} mice (see Supplementary Methods). Females were palpated twice weekly for mammary gland nodules. As soon as tumors appeared, they were routinely measured with external caliper, and volume was calculated as $(4\pi/3) \times (\text{width}/2)^2 \times (\text{length}/2)$. Animals were sacrificed and mammary glands, breast tumors and lungs were collected (see Supplementary Methods) at the following time points: 1)

when the first tumor in each animal appeared, 2) 40 days after the appearance of the first tumor, and 3) 90 days after the appearance of the first tumor.

Additional methods are available in the Supplementary Methods

Results

Elevated CB₂ expression in HER2+ tumors correlates with poor patient prognosis.

In two small cohorts of human samples, we previously reported that CB₂ mRNA expression correlates with higher histological grades and increased HER2 expression (15), and that the CB₂ protein was present in the vast majority of HER2+ tumors (16). Here, we analyzed CB₂ expression in a much larger series of tissue sections [649 breast human samples included in different tissue microarrays (TMAs)]. CB₂ expression was scored as 0 (no staining), 1 (weak staining), 2 (moderate staining) or 3 (high staining) (Figure 1A). We observed that non-tumor breast tissue expressed undetectable levels of CB₂ (Figure 1B). Conversely, CB₂ was expressed by a very large fraction of human breast adenocarcinomas (476 out of 629, i.e. 76%). CB₂ expression was highly associated to HER2+ tumors (Figure 1C, $p=6 \times 10^{-7}$, Pearson's Chi-squared test), while no association between CB₂ expression and hormone-sensitive or triple negative tumors was detected (Figure 1C). Thus, 97% of the HER2+ samples scored positive for CB₂ expression (Figure 1C). Moreover, 65% of them expressed elevated levels of CB₂ (scores 2 and 3) (Figure 1C). Importantly, these HER2+/high CB₂ patients had decreased overall survival (Figure 2A, $p=0.009$, Logrank test), and higher probability to suffer local recurrence (Figure 2B, $p=0.003$, Logrank test) and to develop distant metastases (Figure 2C, $p=0.009$, Logrank test) than HER2+/low CB₂ (scores 0 and 1) patients. Similar observations were made when CB₂ mRNA levels were analyzed in

public DNA microarray datasets (17-19) (Figures 2D-F, $p=0.059$ in D, $p=0.036$ in E, and $p=0.007$ in F, Logrank test). Of interest, this correlation was not observed in HER2- patients (Figures 2G-I). Together, these results show a strong association between CB₂ expression and tumor aggressiveness in HER2+ breast cancer.

The lack of CB₂ impairs breast tumor generation and progression. We next analyzed whether there was a cause and effect link between elevated CB₂ expression and increased aggressiveness in HER2+ tumors. First, we observed that CB₂ expression in the non-cancerous mammary glands of adult wild-type (WT) female mice was virtually undetectable (Supplementary Figures 1A-B). Moreover, it remained very low and unchanged during adult mammary gland development (Supplementary Figures 1A-B). These results suggest that CB₂ may not play a major role in the physiology of the healthy adult mammary gland. Next, we analyzed breast tumor generation and progression in an animal model of HER2-driven breast cancer (the MMTV-neu mouse) in which CB₂ expression was knocked-out (Supplementary Figures 1C-D). MMTV-neu:CB₂^{-/-} mice showed a striking delay in tumor onset as compared with their WT littermates (Figure 3A). Upon early detection, tumor histological features were very similar in both groups (low grade adenocarcinomas with no lymphatic invasion) (Supplementary Figure 1E), the only apparent difference between them being their mitotic index (medium in WT animals and low in the CB₂^{-/-} population) (Supplementary Figure 1E). Forty days after their appearance, 100% of the CB₂ KO-derived tumors kept their original histological characteristics, while 40% of those derived from WT animals were solid carcinomas with necrotic areas (Supplementary Figure 1E). At the final stage of the disease (90 days after tumor appearance), CB₂^{-/-} tumors had negligible changes in their histology (although 40% of them presented necrotic areas), but the WT group

included 40% of solid carcinomas, 40% of tumors with necrotic areas and 20% of tumors with evident signs of lymphatic invasion (Supplementary Figure 1E), all of them signs of more aggressive tumors.

The lack of CB₂ receptors also reduced the number of tumors generated per animal (Figure 3B) and slowed-down tumor growth (Figure 3C). The delayed tumor onset and the decreased tumor multiplicity and growth associated to the lack of CB₂ receptors were accompanied by reduced levels of cyclin D1 and increased levels of the CDK inhibitor p21 in the tumors (Figures 3D-E), both of which are hallmarks of HER2-induced malignant transformation and progression (20-22). In addition, the levels of the endocannabinoid anandamide were higher in CB₂^{-/-}-derived tumors than in CB₂^{+/+} tumors (Supplementary Figure 1F), and the mRNA levels of the enzyme responsible for anandamide degradation (FAAH) were lower in CB₂-deficient tumors than in CB₂ WT lesions (Supplementary Figure 1G). Finally, CB₂ deficiency produced a remarkable reduction in the percentage of animals with lung metastases (Figure 3F). This phenotype correlated with decreased tumor levels of tenascin-C, SPARC, and COX2 (Figure 3G), which have been proposed to mediate metastasis specifically directed to the lungs (23). Together, these results indicate that CB₂ plays an important role in promoting HER2+ breast tumor generation and progression.

HER2 enhances CB₂ expression by activating the transcription factor ELK1 via ERK. Since we observed that virtually all HER2+ human tumors express CB₂ (Figure 1), we analyzed whether HER2 controls the expression of the cannabinoid receptor. Ectopic overexpression of HER2 in triple negative (no estrogen receptor, progesterone receptor and HER2 expression) MDA-MB-231 cells resulted in an increased transcription of CB₂ (Figure 4A). The *in silico* analysis of the CB₂ promoter sequence

revealed the existence of, among others, several ELK1-binding sites (24) (Figure 4B). ELK1 belongs to the ETS transcription factor family, which has been related to cancer (25), and is a well-established target of the ERK cascade (26). We observed that HER2 overexpression activated ELK1, an effect that was accompanied by the activation of ERK (Figure 4C). Of interest, incubation with the MEK inhibitor U0126 prevented the enhancement of p-ELK1 levels (Figure 4C). Moreover, pharmacological inhibition of MEK (Figure 4D) and genetic knock-down of ELK1 (Figure 4E) blocked the increase in CB₂ mRNA levels elicited by HER2 overexpression. In the same line, ELK1 knock-down decreased CB₂ mRNA levels in breast cancer cells that endogenously overexpress HER2, an effect that was not observed in HER2-negative cells (Figure 4F). By chromatin immunoprecipitation assays, we confirmed that ELK1 physically interacts with the CB₂ promoter, and that this interaction is enhanced upon HER2 overexpression and prevented by inhibition of the ERK cascade (Figure 4F). Moreover, ELK1 was able to activate the CB₂ promoter. Thus, transfection of HEK293T cells with a luciferase reporter encoding the CB₂ gene promoter (pGL3- CB₂) together with a constitutively active ELK1-expressing plasmid resulted in an increased luciferase activity when compared to cells transfected with pGL3- CB₂ only (Figure 4G). Point mutations in the CB₂ promoter revealed that the putative ELK1-binding sites located at positions -71 and -89 are the ones responsible for ELK1-induced activation of CB₂ expression (Figure 4G). Together, these observations demonstrate that HER2 promotes CB₂ upregulation by activating the transcription factor ELK1 via ERK activation. Supporting the relevance of this observation, the analysis of 1453 human breast cancer samples from 7 different public DNA microarrays (18, 27-32) showed a strong correlation between ELK1 and CB₂ mRNA expression (Figures 4H-I), and the immunofluorescence analysis

of HER2+ breast cancer biopsies revealed that CB₂-positive cancer cells presented nuclear ELK1 immunoreactivity (Figure 4J).

HER2 forms heteromers with CB₂. We next aimed at determining whether the HER2-CB₂ functional crosstalk was due to a molecular interaction between the receptors.

Immunofluorescence analysis of human HER2+ breast cancer cells revealed that the two receptors colocalize (Figure 5A). Moreover, immunoprecipitation of HER2 in HEK cells produced the co-precipitation of CB₂, and *vice versa* (Figure 5B). The HER2-CB₂ molecular association in cancer cells was confirmed using the proximity ligation assay. Thus, ectopic overexpression of HER2 in MDA-MB-231 cells enhanced the levels of CB₂ (Figure 5C), and this effect was accompanied by the appearance of fluorescent dots, i.e. HER2-CB₂ heteromers (Figure 5D). This fluorescent signal was not evident either in cells that do not express HER2 (with very low levels of CB₂) or in cells in which CB₂ expression was knocked-down by means of selective shRNA (Figure 5D). Importantly, the presence of HER2/CB₂ heterodimers was detected in human breast cancer cells that endogenously overexpress HER2 (Figure 5E) and in HER2-positive human breast cancer tissue (Figure 5F). Again, the heteromer fluorescent signal was not evident either when CB₂ was stably silenced in cells (Figure 5E) or in tumors that do not overexpress HER2 (Figure 5F). These results confirm that CB₂ is upregulated by HER2 and support that HER2 and CB₂ form heteromers in cancer cells.

CB₂ overexpression confers pro-oncogenic advantages on HER2+ breast cancer cells. We next analyzed the biological consequences of the HER2-induced CB₂ upregulation. HER2 overexpression in MDA-MB-231 cells (which effectively enhanced CB₂ levels, Figure 5C) increased cancer cell viability (Figure 6A) and stimulated

properties of cancer cells intimately related to tumor progression, i.e. anchorage-independent growth (Figure 6B) and invasion (Figure 6C). These effects were prevented by CB₂ knock-down (Figures 6A-C). In the same line, genetic silencing of CB₂ (Supplementary Figure 1H) reduced cell viability (Figure 6D), cell invasion (Figure 6E), colony formation in soft agar (Figure 6F) and the expression of metastasis markers (Supplementary Figure 1I) in cells endogenously overexpressing HER2, an effect that was not observed in HER2-negative cells. Moreover, the growth of MDA-MB-231 HER2-overexpressing orthotopic xenografts (Figures 6G-H) and the generation of lung metastases (Figures 6I-L) were significantly impaired upon stable CB₂ knock-down. Similarly, tumors generated from HER2-amplified cells significantly reduced their growth when CB₂ was silenced (Figure 6M). Collectively, these data show that CB₂ promotes pro-oncogenic responses in a HER2+ context.

CB₂ favors HER2-induced activation of c-SRC. Next, we aimed at identifying CB₂ targets responsible for its pro-tumoral activity. Upon modulation of CB₂ and HER2 expression, and by means of a phospho-kinase array, we detected significant alterations in some members of the SRC family of non-receptor tyrosine kinases, which has been extensively related to cancer (33-35). Specifically, we found that the expression of phosphorylated LYN, LCK, YES, FGR, HCK and FYN decreased upon CB₂ knock-down (Figures 7A-B). However, this effect was observed both in HER2+ and HER2- cells (Figure 7A-B), which suggests that, although these may be relevant CB₂ targets in breast cancer, they are not HER2+ context-specific. Of interest, the phosphorylated form of another member of the SRC family (c-SRC), which has particular relevance in cancer development and progression (33), was specifically upregulated upon HER2 overexpression and downregulated by CB₂ knock-down in that high-HER2 context

(Figures 7B-C). Moreover, when CB₂ expression was restored in MDA-MB-231-HER2 shCB₂ cells, p-c-SRC levels were increased, an effect that was not evident in the MDA-MB-231 that do not overexpress HER2 (Figure 7D). In the same line, a decrease in p-c-SRC upon CB₂ silencing was observed in a panel of 5 breast cancer cell lines that endogenously overexpress HER2 (Figure 7E).

Next, we tested whether c-SRC was responsible for CB₂-driven oncogenesis. First, we observed that mouse NIH/3T3 embryonic fibroblasts acquire clonogenic properties upon overexpression of either CB₂ or HER2 (Figures 8A-B). Moreover, the ability of these cells to form colonies in soft agar significantly increased when the two receptors were simultaneously overexpressed (Figures 8A-B). Disruption of c-SRC signaling by using a c-SRC dominant negative construct prevented the oncogenic phenotype induced by CB₂ plus HER2 (Figures 8A-B). Of interest, while the HER2-mediated increased clonogenicity was prevented by blocking c-SRC signaling, the CB₂-induced clonogenic response was not (Figures 8A-B), which indicates that CB₂ promotes c-SRC activation (and the subsequent clonogenic response) via HER2. We then performed colony formation experiments with human HER2-amplified breast cancer cells. Specifically, we overexpressed CB₂ in 5 HER2+ cell lines and observed an increase in the levels of p-c-SRC (Figure 8C). As expected, this increase in activated c-SRC was accompanied by an enhanced clonogenicity (Figure 8D). Importantly, pharmacological inhibition of c-SRC with Saracatinib (a SRC family kinase/Abl dual-kinase inhibitor) in CB₂-overexpressing cells kept both clonogenicity (Figure 8D) and p-c-SRC expression (Figure 8C) at the same level than in pcDNA3-transfected cells treated with the inhibitor, which again suggests that CB₂-driven oncogenesis is mediated by activation of c-SRC. Finally, and in further support of a causal link between the CB₂/HER2/c-SRC axis and pro-oncogenic events, we found a decreased c-

SRC and AKT activation in tumors generated by CB₂-deficient animals [which present a less aggressive phenotype (Figure 3)] with respect to their WT littermates (Figures 8E and 8F), and the analysis of human tumor biopsies revealed that HER2+ breast cancer cells expressing activated c-SRC also expressed CB₂ (Figure 8G).

Discussion

Here we demonstrate not only that the cannabinoid receptor CB₂ exerts a remarkable pro-oncogenic function in HER2+ breast cancer, but also that CB₂ plays a pivotal role in HER2-mediated pro-oncogenic signaling (Figure 8H). It is widely accepted that GPCRs and TKRs control critical biological processes intimately related to oncogenesis, and that the functional crosstalk between members of these two receptor superfamilies (e.g. transactivation of TKRs by GPCR-mediated signaling) may have important consequences in the progression and resistance to TKR-targeted therapies of some types of cancer (36, 37), including HER2+ breast cancer (38). In some cases, the functional crosstalk between GPCRs and TKRs might rely on a physical interaction between receptors. Regarding HER2 specifically, it has been reported that this receptor can form a complex with the β₂-adrenergic receptor in the heart and brain, which is required for mitogen-activated protein kinase activation induced by multiple GPCR agonists in cardiac myocytes (39). Here we show for the first time that a TKR (HER2) forms heteromers with a GPCR (CB₂) in cancer cells. **These findings reveal an unprecedented mechanism of control of HER2 activity that involves cannabinoid receptor CB₂, and suggest that the simultaneous targeting of the two receptors (or common downstream effectors) may be a reasonable therapeutic strategy.** Since dual-targeting approaches are showing positive results in preclinical and clinical contexts when the targets are different members of the ERBB family (mainly ERBB1 and ERBB2) or even different

domains of the same receptor (neutralizing antibodies + tyrosine kinase inhibitors, for example) (40), it is tempting to speculate that the combination of anti-HER2 compounds with cannabinoids targeting CB₂ may have synergistic antitumoral effects. Interestingly, there is evidence showing that, at least at the preclinical level, the combination of cannabinoids with other anticancer therapies results in improved responses when compared with the corresponding individual treatments (11, 41-44). In any case, further studies should be performed to unveil the functional relevance of the HER2-CB₂ heteromers.

Our findings also show that the non-receptor tyrosine kinase c-SRC plays a pivotal role in CB₂-induced HER2 pro-oncogenic signaling (Figure 7). c-SRC promotes cell proliferation, survival, migration and angiogenesis (33), and its deregulation is associated with oncogenesis (34, 35) and poor patient prognosis (45). Together, these features made c-SRC an excellent target for the clinical development of specific inhibitors (34, 35, 45, 46). In HER2+ breast cancer in particular, c-SRC activation has been implicated in the generation of brain metastases (47), a condition that has no curative treatment, and in the development of trastuzumab resistance (48). Interestingly, treatment of brain metastasis-bearing mice with a combination of Lapatinib (which targets ERBB1 and ERBB2) and a c-SRC inhibitor slowed-down the growth of the metastases (47), and treatment of trastuzumab-resistant cells/tumors with a c-SRC inhibitor restored trastuzumab resistance (48). These data suggest that blocking c-SRC may be an effective manner to treat two important remaining clinical challenges in HER2+ breast cancer: the treatment of highly metastatic tumors (especially those colonizing the central nervous system) and trastuzumab resistance (both innate and acquired). Additional experiments should be performed to analyze the involvement of CB₂ in c-SRC-mediated trastuzumab resistance and generation of brain metastasis.

Our results clearly reveal a pro-oncogenic role of CB₂ in HER2+ breast cancer. However, it has been widely described that pharmacological activation of this particular receptor exerts antitumoral effects in different models of breast (15, 16, 49, 50) and many other types of cancer (11). Further experiments should be performed to get a deeper insight into the molecular details of this bimodal effect of CB₂ receptor functionality. For example, it would be interesting to know whether different cannabinoid stimuli (i.e. an endogenous tone *vs* an exogenous pharmacological activation) produce a different activation of CB₂/HER2-mediated signaling in terms of intensity and/or specific pathways.

Finally, we have observed a strong association between higher CB₂ protein expression in HER2+ breast tumors and lower patient overall, relapse-free and metastasis-free survival. It has been previously shown that the levels of CB₂ are elevated in breast (15, 16, 50) and many other types of cancer compared to healthy matching tissue (11), and in the more aggressive (high grade) breast (15, 16) and brain (51-53) tumors compared to the respective less aggressive (low grade) tumors. Recently, an association between CB₂ expression and overall and disease-free survival of patients with squamous cell carcinoma of the head and neck has also been reported (54). All these observations may serve to exploit CB₂ as a new prognostic marker in oncology (at least in certain types of tumors).

References

1. Curtis C, Shah SP, Chin SF, et al. The genomic and transcriptomic architecture of 2,000 breast tumours reveals novel subgroups. *Nature*. 2012;486(7403):346-52.
2. Perou CM, Sorlie T, Eisen MB, et al. Molecular portraits of human breast tumours. *Nature*. 2000;406(6797):747-52.
3. Sorlie T, Perou CM, Tibshirani R, et al. Gene expression patterns of breast carcinomas distinguish tumor subclasses with clinical implications. *Proc Natl Acad Sci U S A*. 2001;98(19):10869-74.
4. Sotiriou C, Neo SY, McShane LM, et al. Breast cancer classification and prognosis based on gene expression profiles from a population-based study. *Proc Natl Acad Sci U S A*. 2003;100(18):10393-8.
5. Higgins MJ, Baselga J. Targeted therapies for breast cancer. *J Clin Invest*. 2011;121(10):3797-803.
6. Moasser MM. The oncogene HER2: its signaling and transforming functions and its role in human cancer pathogenesis. *Oncogene*. 2007;26(45):6469-87.
7. Pacher P, Batkai S, Kunos G. The endocannabinoid system as an emerging target of pharmacotherapy. *Pharmacol Rev*. 2006;58(3):389-462.
8. Pertwee RG, Howlett AC, Abood ME, et al. International Union of Basic and Clinical Pharmacology. LXXIX. Cannabinoid receptors and their ligands: beyond CB and CB. *Pharmacol Rev*. 2010;62(4):588-631.
9. Fowler CJ, Gustafsson SB, Chung SC, et al. Targeting the endocannabinoid system for the treatment of cancer--a practical view. *Curr Top Med Chem*. 2010;10(8):814-27.
10. Guzman M. Cannabinoids: potential anticancer agents. *Nat Rev Cancer*. 2003;3(10):745-55.

11. Velasco G, Sanchez C, Guzman M. Towards the use of cannabinoids as antitumour agents. *Nat Rev Cancer*. 2012;12(6):436-44.
12. Alpini G, Demorrow S. Changes in the endocannabinoid system may give insight into new and effective treatments for cancer. *Vitam Horm*. 2009;81:469-85.
13. Pisanti S, Bifulco M. Endocannabinoid system modulation in cancer biology and therapy. *Pharmacol Res*. 2009;60(2):107-16.
14. Guindon J, Hohmann AG. The endocannabinoid system and cancer: therapeutic implication. *Br J Pharmacol*. 2011;163(7):1447-63.
15. Caffarel MM, Sarrio D, Palacios J, et al. Delta9-tetrahydrocannabinol inhibits cell cycle progression in human breast cancer cells through Cdc2 regulation. *Cancer Res*. 2006;66(13):6615-21.
16. Caffarel MM, Andradas C, Mira E, et al. Cannabinoids reduce ErbB2-driven breast cancer progression through Akt inhibition. *Mol Cancer*. 2010;9:196.
17. Bild AH, Yao G, Chang JT, et al. Oncogenic pathway signatures in human cancers as a guide to targeted therapies. *Nature*. 2006;439(7074):353-7.
18. Chin K, DeVries S, Fridlyand J, et al. Genomic and transcriptional aberrations linked to breast cancer pathophysiologies. *Cancer Cell*. 2006;10(6):529-41.
19. Gyorffy B, Lanczky A, Eklund AC, et al. An online survival analysis tool to rapidly assess the effect of 22,277 genes on breast cancer prognosis using microarray data of 1,809 patients. *Breast Cancer Res Treat*. 2010;123(3):725-31.
20. Yu Q, Geng Y, Sicinski P. Specific protection against breast cancers by cyclin D1 ablation. *Nature*. 2001;411(6841):1017-21.
21. Cheng X, Xia W, Yang JY, et al. Activation of p21(CIP1/WAF1) in mammary epithelium accelerates mammary tumorigenesis and promotes lung metastasis. *Biochem Biophys Res Commun*. 2010;403(1):103-7.

22. Muraoka RS, Lenferink AE, Law B, et al. ErbB2/Neu-induced, cyclin D1-dependent transformation is accelerated in p27-haploinsufficient mammary epithelial cells but impaired in p27-null cells. *Mol Cell Biol.* 2002;22(7):2204-19.
23. Minn AJ, Gupta GP, Siegel PM, et al. Genes that mediate breast cancer metastasis to lung. *Nature.* 2005;436(7050):518-24.
24. Treisman R, Marais R, Wynne J. Spatial flexibility in ternary complexes between SRF and its accessory proteins. *EMBO J.* 1992;11(12):4631-40.
25. Seth A, Watson DK. ETS transcription factors and their emerging roles in human cancer. *Eur J Cancer.* 2005;41(16):2462-78.
26. Janknecht R, Hunter T. Convergence of MAP kinase pathways on the ternary complex factor Sap-1a. *EMBO J.* 1997;16(7):1620-7.
27. Desmedt C, Piette F, Loi S, et al. Strong time dependence of the 76-gene prognostic signature for node-negative breast cancer patients in the TRANSBIG multicenter independent validation series. *Clin Cancer Res.* 2007;13(11):3207-14.
28. Hatzis C, Pusztai L, Valero V, et al. A genomic predictor of response and survival following taxane-anthracycline chemotherapy for invasive breast cancer. *JAMA.* 2011;305(18):1873-81.
29. Loi S, Haibe-Kains B, Desmedt C, et al. Definition of clinically distinct molecular subtypes in estrogen receptor-positive breast carcinomas through genomic grade. *J Clin Oncol.* 2007;25(10):1239-46.
30. Miller LD, Smeds J, George J, et al. An expression signature for p53 status in human breast cancer predicts mutation status, transcriptional effects, and patient survival. *Proc Natl Acad Sci U S A.* 2005;102(38):13550-5.
31. Minn AJ, Gupta GP, Padua D, et al. Lung metastasis genes couple breast tumor size and metastatic spread. *Proc Natl Acad Sci U S A.* 2007;104(16):6740-5.

32. Pawitan Y, Bjohle J, Amler L, et al. Gene expression profiling spares early breast cancer patients from adjuvant therapy: derived and validated in two population-based cohorts. *Breast Cancer Res.* 2005;7(6):R953-64.
33. Yeatman TJ. A renaissance for SRC. *Nat Rev Cancer.* 2004;4(6):470-80.
34. Zhang S, Yu D. Targeting Src family kinases in anti-cancer therapies: turning promise into triumph. *Trends Pharmacol Sci.* 2012;33(3):122-8.
35. Kim LC, Song L, Haura EB. Src kinases as therapeutic targets for cancer. *Nat Rev Clin Oncol.* 2009;6(10):587-95.
36. Almendro V, Garcia-Recio S, Gascon P. Tyrosine kinase receptor transactivation associated to G protein-coupled receptors. *Curr Drug Targets.* 2010;11(9):1169-80.
37. Pyne NJ, Pyne S. Receptor tyrosine kinase-G-protein-coupled receptor signalling platforms: out of the shadow? *Trends Pharmacol Sci.* 2011;32(8):443-50.
38. Li YM, Pan Y, Wei Y, et al. Upregulation of CXCR4 is essential for HER2-mediated tumor metastasis. *Cancer Cell.* 2004;6(5):459-69.
39. Negro A, Brar BK, Gu Y, et al. erbB2 is required for G protein-coupled receptor signaling in the heart. *Proc Natl Acad Sci U S A.* 2006;103(43):15889-93.
40. Tebbutt N, Pedersen MW, Johns TG. Targeting the ERBB family in cancer: couples therapy. *Nat Rev Cancer.* 2013;13(9):663-73.
41. Donadelli M, Dando I, Zaniboni T, et al. Gemcitabine/cannabinoid combination triggers autophagy in pancreatic cancer cells through a ROS-mediated mechanism. *Cell Death Dis.* 2011;2:e152.
42. Miyato H, Kitayama J, Yamashita H, et al. Pharmacological synergism between cannabinoids and paclitaxel in gastric cancer cell lines. *J Surg Res.* 2009;155(1):40-7.

43. Torres S, Lorente M, Rodriguez-Fornes F, et al. A combined preclinical therapy of cannabinoids and temozolomide against glioma. *Mol Cancer Ther.* 2011;10(1):90-103.
44. Gustafsson SB, Lindgren T, Jonsson M, et al. Cannabinoid receptor-independent cytotoxic effects of cannabinoids in human colorectal carcinoma cells: synergism with 5-fluorouracil. *Cancer Chemother Pharmacol.* 2009;63(4):691-701.
45. Wheeler DL, Iida M, Dunn EF. The role of Src in solid tumors. *Oncologist.* 2009;14(7):667-78.
46. Aleshin A, Finn RS. SRC: a century of science brought to the clinic. *Neoplasia.* 2010;12(8):599-607.
47. Zhang S, Huang WC, Zhang L, et al. SRC family kinases as novel therapeutic targets to treat breast cancer brain metastases. *Cancer Res.* 2013;73(18):5764-74.
48. Zhang S, Huang WC, Li P, et al. Combating trastuzumab resistance by targeting SRC, a common node downstream of multiple resistance pathways. *Nat Med.* 2011;17(4):461-9.
49. Ligresti A, Moriello AS, Starowicz K, et al. Antitumor activity of plant cannabinoids with emphasis on the effect of cannabidiol on human breast carcinoma. *J Pharmacol Exp Ther.* 2006;318(3):1375-87.
50. Qamri Z, Preet A, Nasser MW, et al. Synthetic cannabinoid receptor agonists inhibit tumor growth and metastasis of breast cancer. *Mol Cancer Ther.* 2009;8(11):3117-29.
51. Calatuzzolo C, Salmaggi A, Pollo B, et al. Expression of cannabinoid receptors and neurotrophins in human gliomas. *Neurol Sci.* 2007;28(6):304-10.

52. Ellert-Miklaszewska A, Grajkowska W, Gabrusiewicz K, et al. Distinctive pattern of cannabinoid receptor type II (CB2) expression in adult and pediatric brain tumors. *Brain Res.* 2007;1137(1):161-9.
53. Sanchez C, de Ceballos ML, Gomez del Pulgar T, et al. Inhibition of glioma growth in vivo by selective activation of the CB(2) cannabinoid receptor. *Cancer Res.* 2001;61(15):5784-9.
54. Klein Nulent TJ, Van Diest PJ, van der Groep P, et al. Cannabinoid receptor-2 immunoreactivity is associated with survival in squamous cell carcinoma of the head and neck. *Br J Oral Maxillofac Surg.* 2013;51(7):604-9.

Funding

This work was supported by grants from Spanish Ministry of Economy and Competitiveness (PI11/00295 to CS, SAF2012-36566 to JF-P, SAF2010-22198 to SO-G and Ramón y Cajal fellowship to PJM); GW Pharmaceuticals (to CS); Madrid Regional Government (S2010/BMD-2308 to MG, S2010/BMD-2353 to SO-G and S2011/BMD-2470 to JF-P); Fundación Mutua Madrileña; and Instituto de Salud Carlos III (CIBERER-3-749/172.03 to JF-P). EP-G and EM-V are recipients of Postdoctoral Research Contracts from Fundación Científica Asociación Española Contra el Cáncer. MA is a recipient of a FPU fellowship (from Spanish Ministry of Economy and Competitiveness) and EP-G was a recipient of a FEBS Short-term Fellowship.

Acknowledgements

We are indebted to the members of our laboratories for critical discussion on this work, and especially to Dr. Cerutti and Dr. Hernández-Tiedra for their help in animal experiments. Genotyping services were provided by Centro Nacional de Genotipado - Instituto de Salud Carlos III (CeGen-ISCIII; www.cegen.org).

Affiliations of authors

Dept. Biochemistry and Molecular Biology I, School of Biology, Complutense University, Madrid, Spain (EP-G, CA, MMC, SB-B, EG-T, MG, CS); Instituto de Investigación Hospital 12 de Octubre, Madrid, Spain (EP-G, CA, SB-B, CS). Present address: Dept. Pathology, University of Cambridge, Cambridge, UK (MMC). Centro de Biología Molecular Severo Ochoa, Consejo Superior de Investigaciones Científicas-Universidad Autónoma de Madrid, Madrid, Spain (MV-M, JF-P). Centro de Investigación Biomédica en Red de Enfermedades Raras (CIBERER), Madrid, Spain (MV-M, JF-P). Instituto de Investigación Sanitaria Fundación Jiménez Díaz, Madrid, Spain (MV-M, JF-P). Dept. Biochemistry and Molecular Biology, University of Barcelona, Barcelona, Spain (EM, EIC, PJM). Centro de Investigación Biomédica en Red de Enfermedades Neurodegenerativas (CIBERNED), Madrid, Spain (EM, EIC, PJM, MG). Institute of Biomedicine of the University of Barcelona, Barcelona, Spain (EM, EIC, PJM). Dept. Gynecology and Obstetrics, University Hospital Schleswig-Holstein, Kiel, Germany (SH, AW, IA, MB, NA). Dept. Animal Surgery and Medicine, School of Veterinary, Complutense University, Madrid, Spain (JMF). Instituto de Investigaciones Biomédicas Alberto Sols, Consejo Superior de Investigaciones Científicas-Universidad Autónoma de Madrid, Madrid, Spain (EM-V, GM-B, MQ). Institute of Pathology, University Hospital Schleswig-Holstein, Kiel, Germany (WK, CR). Institute of Pathology, University of Freiburg, Freiburg, Germany (PB). Dept. Gynecology and Obstetrics, University of Freiburg, Freiburg, Germany (ES). Institute of Pathology and Neuropathology, University Hospital of Tübingen, Tübingen, Germany (AS). Spanish National Cancer Research Centre (CNIO), Madrid, Spain (JS, MP-M, DM). Fundación MD Anderson Internacional, Madrid, Spain (GM-B). Dept.

Organic Chemistry, School of Chemistry, Complutense University, Madrid, Spain (SO-G, MA, HV-V). School of Pharmacy, University of East Anglia, Norwich Research Park, Norwich, UK (PJM).

Figure legends

Figure 1. CB₂ expression associates with HER2+ breast tumors. **A)** Representative images showing CB₂ expression scoring according to intensity staining in tissue microarray (TMA) samples: scores 0, 1, 2 and 3 correspond to no, low, moderate and high staining, respectively. **B)** Representative CB₂ immunohistochemical staining in a human non-tumor breast tissue sample included in the analyzed TMAs. Inset, CB₂ staining (brown) in a macrophage is shown as a CB₂ staining-positive control. **C)** Association between CB₂ expression (as determined by staining scoring) and the molecular features of breast tumor samples included in the TMAs. The Pearson's chi-squared test was used for statistical analysis.

Figure 2. Elevated CB₂ expression in HER2+ breast tumors correlates with poor patient prognosis. Kaplan-Meier curves for overall survival (**A, D-G**), survival with no recurrence in the breast (**B and H**) and metastasis-free survival (**C and I**). Data plotted in panels **A-C** correspond to the 65 HER2+ samples included in TMA # 2 (see Methods). Data plotted in panels **G-I** correspond to the 224 HER2- samples included in TMA # 2. Data plotted in panels **D** and **E** were obtained from the microarray data sets published in ArrayExpress database (accession number E-TABM-158) (**D**) and GEO database (accession number GSE3143) (**E**). Data plotted in **F** were obtained from (19) through the Kaplan-Meier Plotter (www.kmplot.com). Survival curves were statistically compared by the Logrank test.

Figure 3. The lack of CB₂ impairs breast tumor generation and progression. **A)** Kaplan-Meier curves for tumor onset in MMTV-neu:CB₂ WT and MMTV-neu:CB₂ KO mice. Results were analyzed by the Pearson's chi-squared test. **B)** Number of tumors

generated per animal 90 days after first tumor arousal. **C)** Tumor volume 70 days after tumor appearance. **D)** Western blot analysis of Cyclin D1 and p21 in tumors generated by the indicated animals. Three representative samples per experimental group are shown. **E)** Densitometric analysis of the levels of the indicated proteins (determined by Western blot; n=7 for MMTV-neu:CB₂ WT tumors and n=6 for MMTV-neu:CB₂ KO tumors). Results are expressed in arbitrary units. **F)** Percentage of animals with lung metastases 90 days after tumor arousal. Lung tumor masses were classified as macrometastases when they were visible to the naked eye at dissection, and as micrometastases when they were only detectable by H&E staining. **G)** mRNA levels (as determined by real-time quantitative PCR) of Tenascin C, SPARC and COX2 in tumors generated by the indicated mice. Results are expressed in arbitrary units. **Except in A,** **data were analyzed by ANOVA with a post-hoc analysis by the Student–Newman–Keuls’ test.** *, p<0,05; **, p <0,01 vs MMTV-neu:CB₂ WT mice.

Figure 4. HER2 enhances CB₂ expression by activating the transcription factor ELK1 via ERK. **A)** ERBB2/HER2 protein expression (upper panel) and CB₂ mRNA expression (lower panel) in MDA-MB-231-HER2 (231-HER2) and MDA-MB-231 cells (231). **B)** **Schematic representation of the CB₂ gene promoter sequence. The positions and sequences of the putative ELK1-binding sites are indicated.** **C)** Western blot analysis of the indicated proteins, in the presence or in the absence of the MEK inhibitor U0126 (5 μM). **D-E)** CB₂ mRNA expression (in arbitrary units), in the presence/absence of U0126 (**D**), or after transfection with ELK1 siRNAs (siELK1) or with a non-targeted siRNA (siC) (**E**). **F)** **Effect of ELK1 knock-down on CB₂ mRNA expression (top panel) in different human breast cancer cells endogenously overexpressing (black bars) or not (gray bars) HER2. Results are expressed in arbitrary**

units vs the corresponding cells transfected with a control siRNA (siC), set at 1 in all cases (white bar). The bottom panel shows the ELK1 mRNA levels found in the cells after ELK1 silencing. **G)** ChIP assay in cells treated with or without U0126. Immunoprecipitation was performed with an anti-ELK1 Ab (or a non-specific rabbit IgG as control). **G)** CB₂ gene promoter activity as determined by a luciferase reporter. Drawings (left) represent the CB₂ promoter construct transfected in each case. A constitutively active ELK1 containing plasmid was always co-transfected with the CB₂ promoter. Line 1, CB₂ promoter empty vector. **H** and **I)** Correlation of CB₂ and ELK1 expression (analyzed by the Pearson's chi-squared test) in human breast cancer samples from 7 public DNA microarrays [(18, 22, 26, 28, 29, 31) in **H** and (28) in **I**]. **J)** Immunofluorescence analysis of CB₂ (green) and phospho-ELK1 (red) in a HER2-positive (upper panels) and a HER2-negative (lower panels) human breast cancer sample. Cell nuclei are stained in blue. Scale bar, 100 μm. Except in I and J, data were analyzed by ANOVA with a post-hoc analysis by the Student–Newman–Keuls' test. **, p<0,01 vs vehicle-treated (**D**) or siC-transfected (**E**) 231 cells; #, p<0,05 vs vehicle-treated (**D**) or siC-transfected (**E**) 231-HER2 cells; **, p<0,01 vs WT (**H**).

Figure 5. HER2 forms heteromers with CB₂. **A)** Immunofluorescence analysis of CB₂ (green) and HER2 (red) protein expression in a HER2-positive (upper panels) and a HER2-negative (lower panels) human breast tumor sample. Cell nuclei are stained in blue. Scale bar, 100 μm. **B)** Analysis of the HER2-CB₂ molecular interaction by immunoprecipitation assay in HEK cells transfected with an ERBB2 overexpression plasmid, a HA-tagged CB₂ plasmid, both of them simultaneously or the corresponding empty vector (pcDNA3). **C)** CB₂ mRNA expression, as determined by real-time quantitative PCR and expressed in arbitrary units, in MDA-MB-231 cells (231) or 231

cells stably overexpressing HER2 (231-HER2), upon stable knock-down of CB₂ with a selective shRNA (shCB₂) pool or after infection with lentiviral particles containing a scrambled shRNA (shC). **D-F**) Proximity ligation assays in 231 shC cells and in 231-HER2 cells infected with either shC or shCB₂ particles (**D**), in BT474 shC and BT474 shCB₂ cells (**E**), and in a HER2-negative and a HER2-positive human breast cancer sample (**F**). Cell nuclei are stained in blue and the red fluorescent signal correspond to CB₂/HER2 heteromers. Scale bars, 20 μm.

Figure 6. CB₂ overexpression confers pro-oncogenic advantages on HER2+ breast cancer cells. **A-F**) Cell viability as determined by the MTT test (**A** and **D**), invasion in matrigel-coated Boyden chambers (**B** and **E**), and number of colonies generated in soft agar (**C** and **F**) of MDA-MB-231 (231) and MDA-MB-231-HER2 cells (231-HER2) stably expressing a shRNA selectively targeting CB₂ (shCB₂) or a scrambled shRNA (shC) (**A-B**) or of the indicated HER2-positive or HER2-negative cell lines (**D-F**). **G**) Schematic representation of the generation of the orthotopic xenografts analyzed in **H** and **M**. **H** and **M**) Evolution of tumor volume in mice injected with either 231 or 231-HER2 cells stably expressing shCB₂ or shC (**H**), or with the indicated HER2-amplified cells stably expressing the same shRNAs (**M**). **I**) Cartoon representing the generation of the lung metastases analyzed in **K** and **L**, by injection of lung-seeking MDA-MB-231-HER2 cells (231-HER2-LM) stably expressing shCB₂, or a shC, into the mouse lateral tail vein. **J**) CB₂ mRNA expression in shC- and shCB₂-231-HER2-LM cells. **K**) Evaluation of the number of lung metastases generated per animal. **L**) Representative lung bioluminescence images (left panels) and quantification of the luminescence signal (right panel) in the two experimental groups. Data were analyzed by ANOVA with a

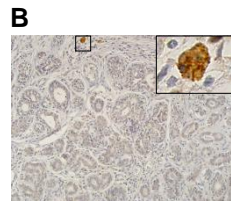
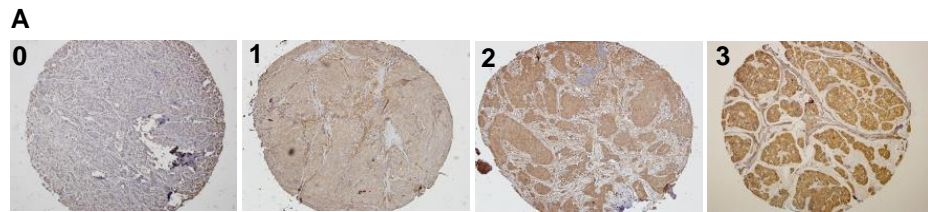
post-hoc analysis by the Student–Newman–Keuls' test. *, p<0,05 and **, p<0,01 vs the corresponding shC cell line; #, p<0,01 vs shC-231-HER2 cells.

Figure 7. Involvement of c-SRC in CB₂-induced HER2-mediated pro-oncogenic signaling. **A)** Phospho-kinase protein array analysis in MDA-MB-231 (231) and MDA-MB-231-HER2 cells (231-HER2) after stable knockdown of CB₂ by means of selective shRNA. Squared dots correspond to the following SRC kinase family members: 1, LYN; 2, LCK; 3, YES; 4, FGR; 5, HCK; 6, c-SRC and 7, FYN. Note that in this phosphoarray kit, each condition consist of two membranes. **B)** Densitometric analysis of the squared dots shown in **A**. **C-E)** Western analysis of the indicated proteins in MDA-MB-231 (231) and MDA-MB-231-HER2 (231-HER2) cells stably expressing a shRNA selectively targeting CB₂ (shCB₂) or a scrambled shRNA (shC) (**C**), or in 231 shCB₂ or 231-HER2 shCB₂ cells stably expressing a HA tagged-CB₂ plasmid (HA-CB₂) or the corresponding empty vector (pcDNA3) (**D**), or in the indicated HER2-amplified cells stably expressing shCB₂ or shC (**E**). Numbers in **E** correspond to the densitometric analysis of the respective bands.

Figure 8. Involvement of c-SRC in CB₂-induced HER2-mediated pro-oncogenic signaling. **A-D)** Anchorage-independent growth (**A** and **D**) and expression of ERBB2, HA-CB₂ and the indicated proteins (**B** and **C**) (as determined by Western blot), in NIH/3T3 fibroblasts (**A** and **B**) and in a panel of 5 HER2+ human breast cancer cell lines (**C** and **D**) transiently transfected with the indicated constructs and/or incubated with 1μM Saracatinib. In **B** and **C** (AU565 cells), lanes were run on the same gel but were noncontiguous. **E** and **F)** Western blot (left panels) and densitometric analysis (right panels) of phospho-c-SRC (**E**) and phosphor-AKT (**F**) in breast tumors generated

by MMTV-neu:CB₂ WT and MMTV-neu:CB₂ KO mice. **G**) Immunofluorescence analysis of CB₂ (green) and phospho-c-SRC (red) in a human HER2+ breast tumor sample. Cell nuclei are stained in blue. Scale bar, 100 μm. **H**) Proposed role of CB₂ in HER2-driven pro-oncogenic signaling: HER2 enhances CB₂ expression by activating the transcription factor ELK1 via ERK. Increased CB₂ expression promotes HER2 pro-oncogenic signaling by activating the tyrosine kinase c-SRC. Data were analyzed by ANOVA with a post-hoc analysis by the Student–Newman–Keuls' test. *, p<0,05 and **, p<0,01 vs pcDNA3; #, p<0,05 vs CB₂ o HER2; &&, p<0,01 vs HER2; \$, p<0,05 vs HER2-CB₂ (**A** and **D**). *, p<0,05 vs MMTV-neu:CB₂ WT mice (**E** and **F**).

Figure 1



		n	CB ₂ staining				p-value
			0	1	2	3	
Hormone receptor status	Positive	504	117 (23%)	191 (38%)	135 (27%)	61 (12%)	0.655
	Negative	117	24 (21%)	41 (35%)	38 (32%)	14 (12%)	
HER2 status	Positive	92	3 (3%)	29 (32%)	39 (42%)	21 (23%)	6x10⁻⁷
	Negative	360	86 (24%)	141 (39%)	94 (26%)	39 (11%)	
Triple negative status	Positive	47	13 (28%)	20 (43%)	12 (26%)	2 (4%)	0.138
	Negative	405	76 (19%)	150 (37%)	121 (30%)	58 (14%)	

Figure 2

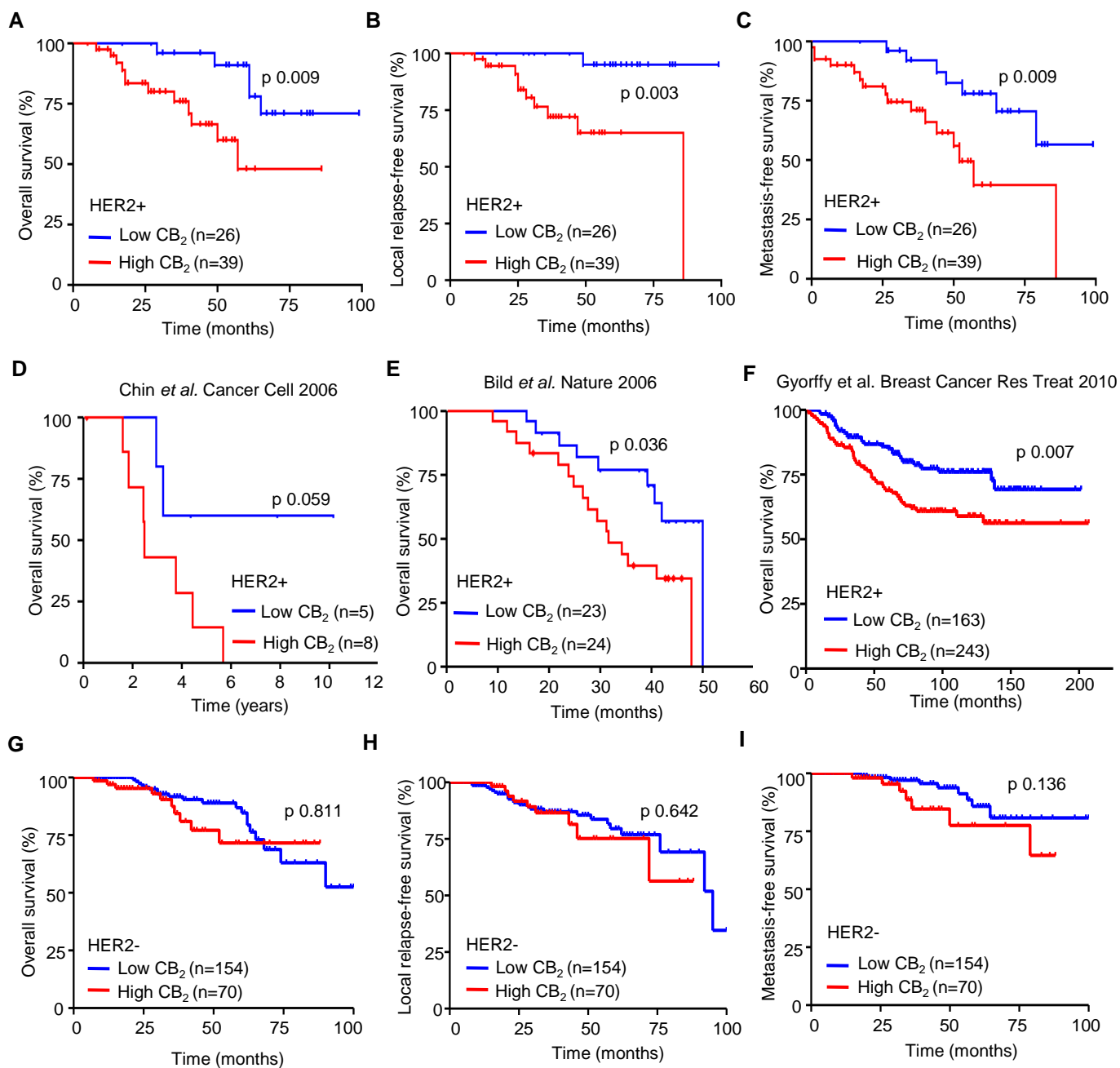


Figure 3

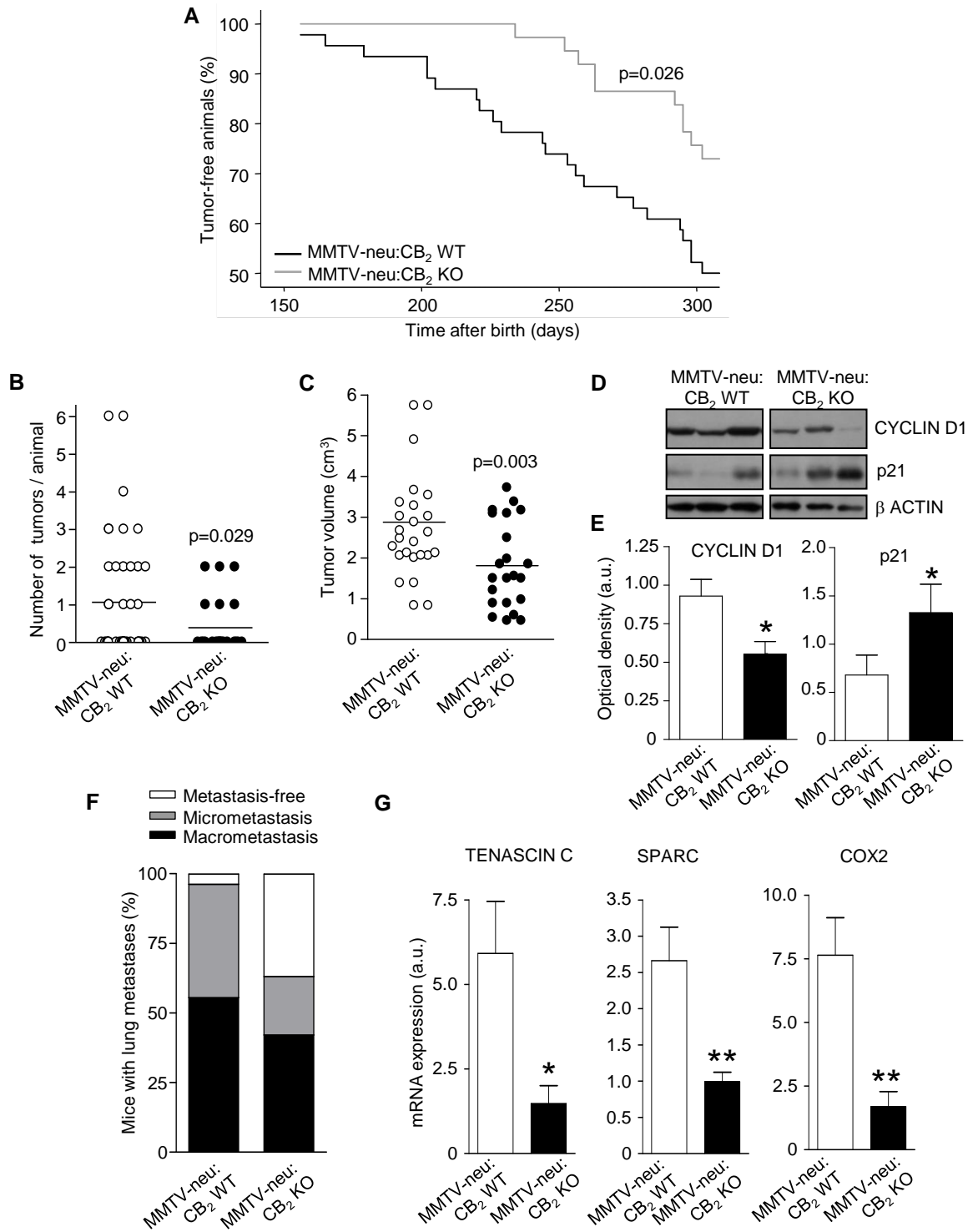


Figure 4

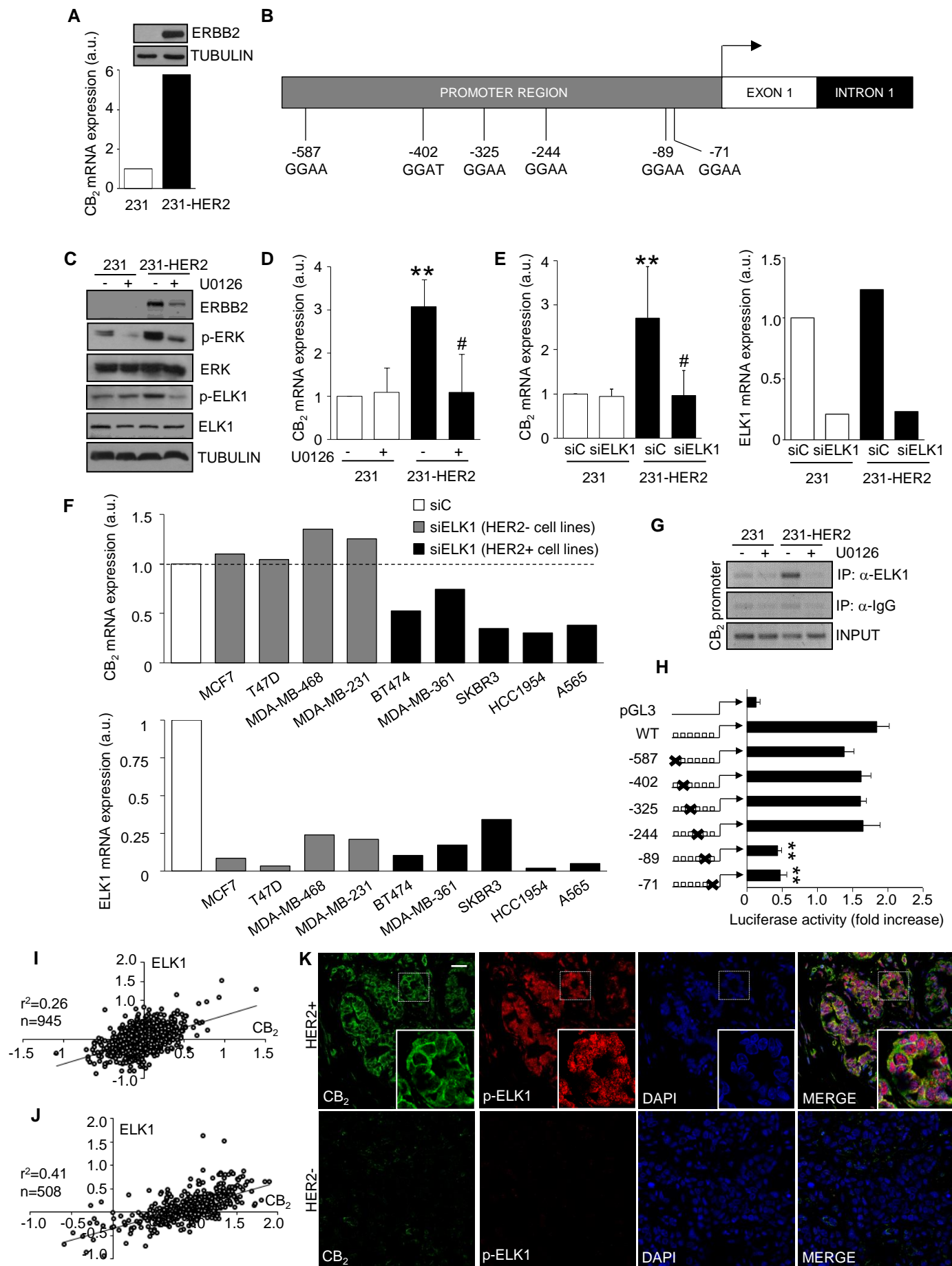


Figure 5

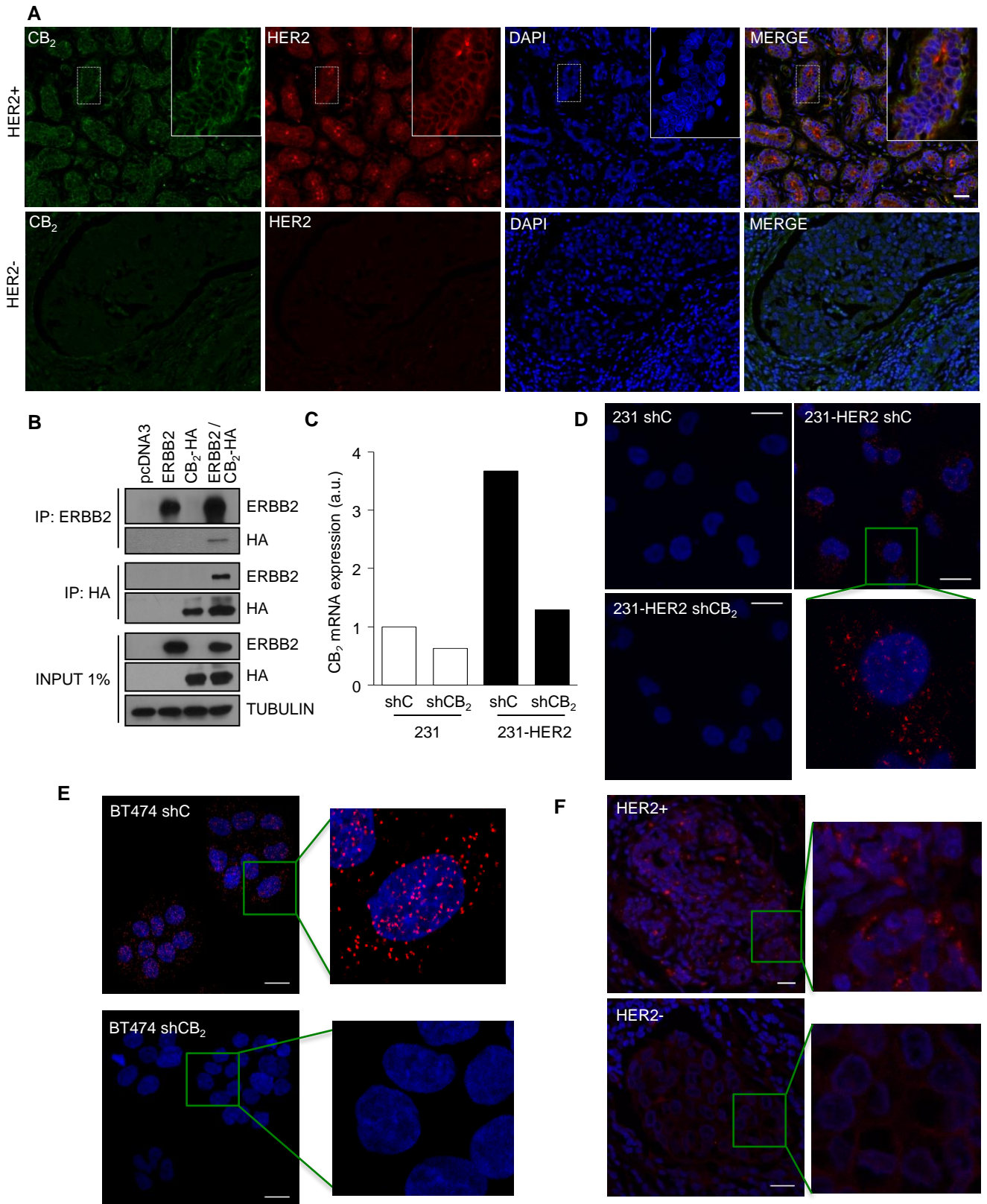


Figure 6

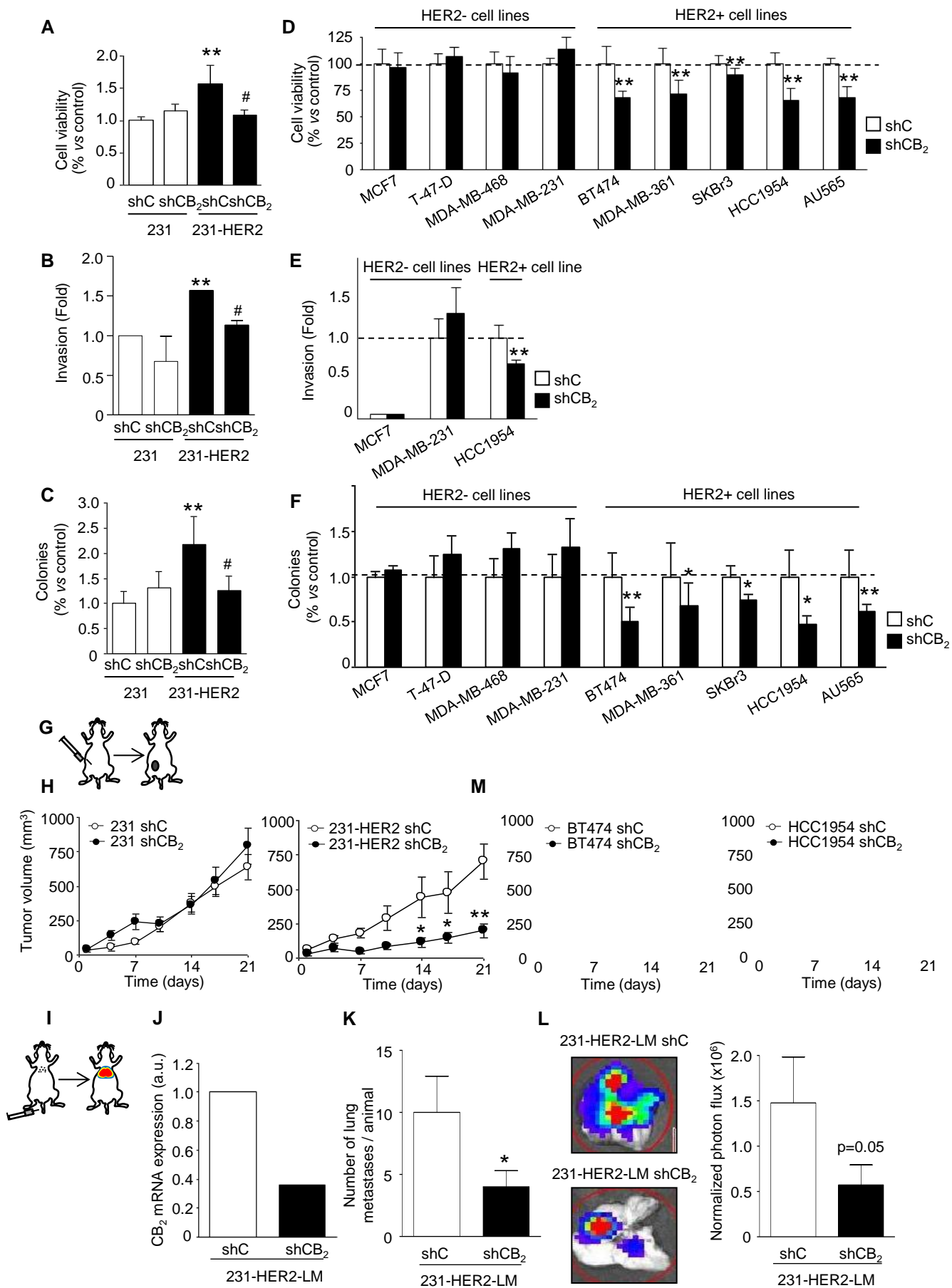


Figure 7

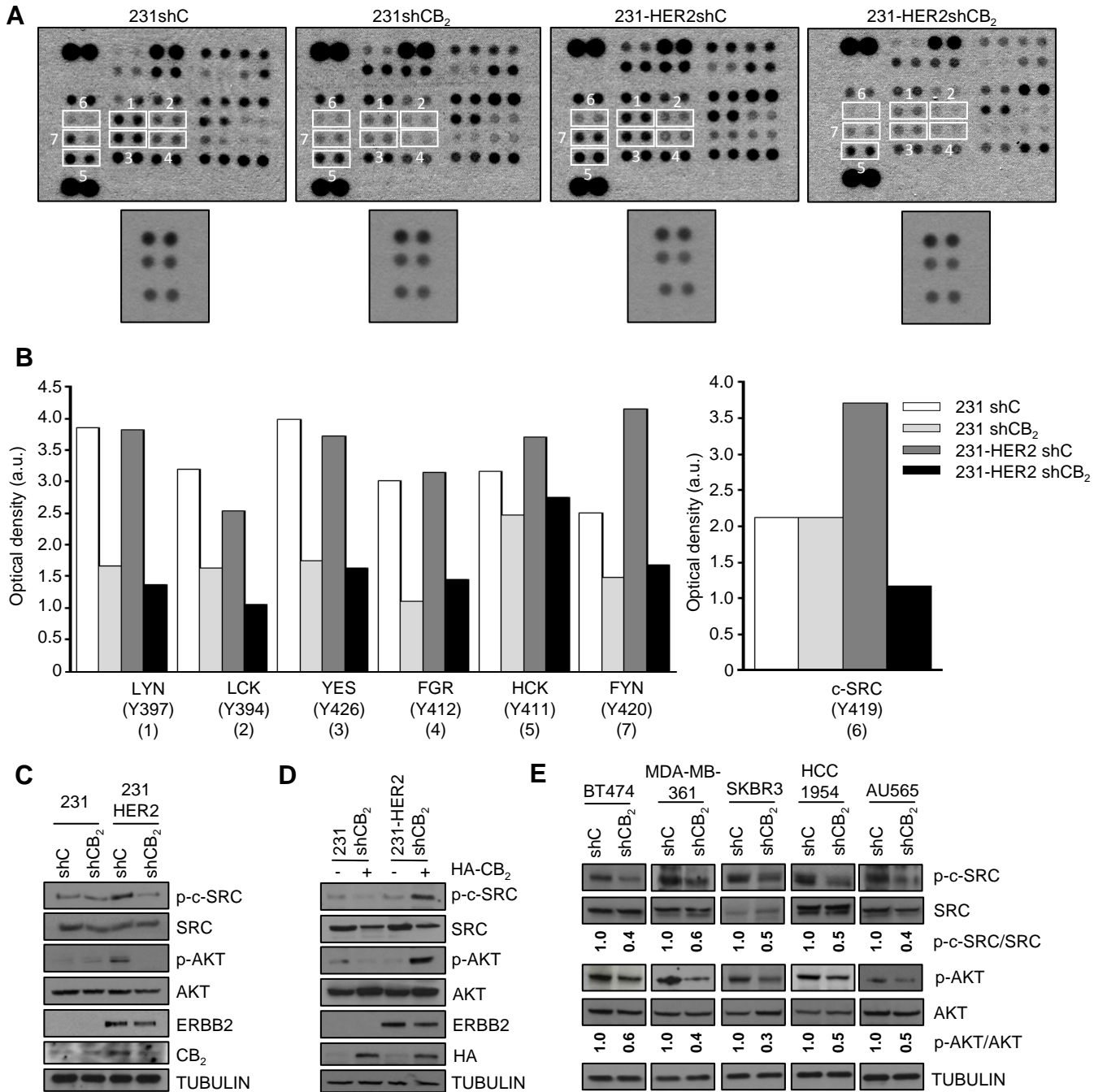
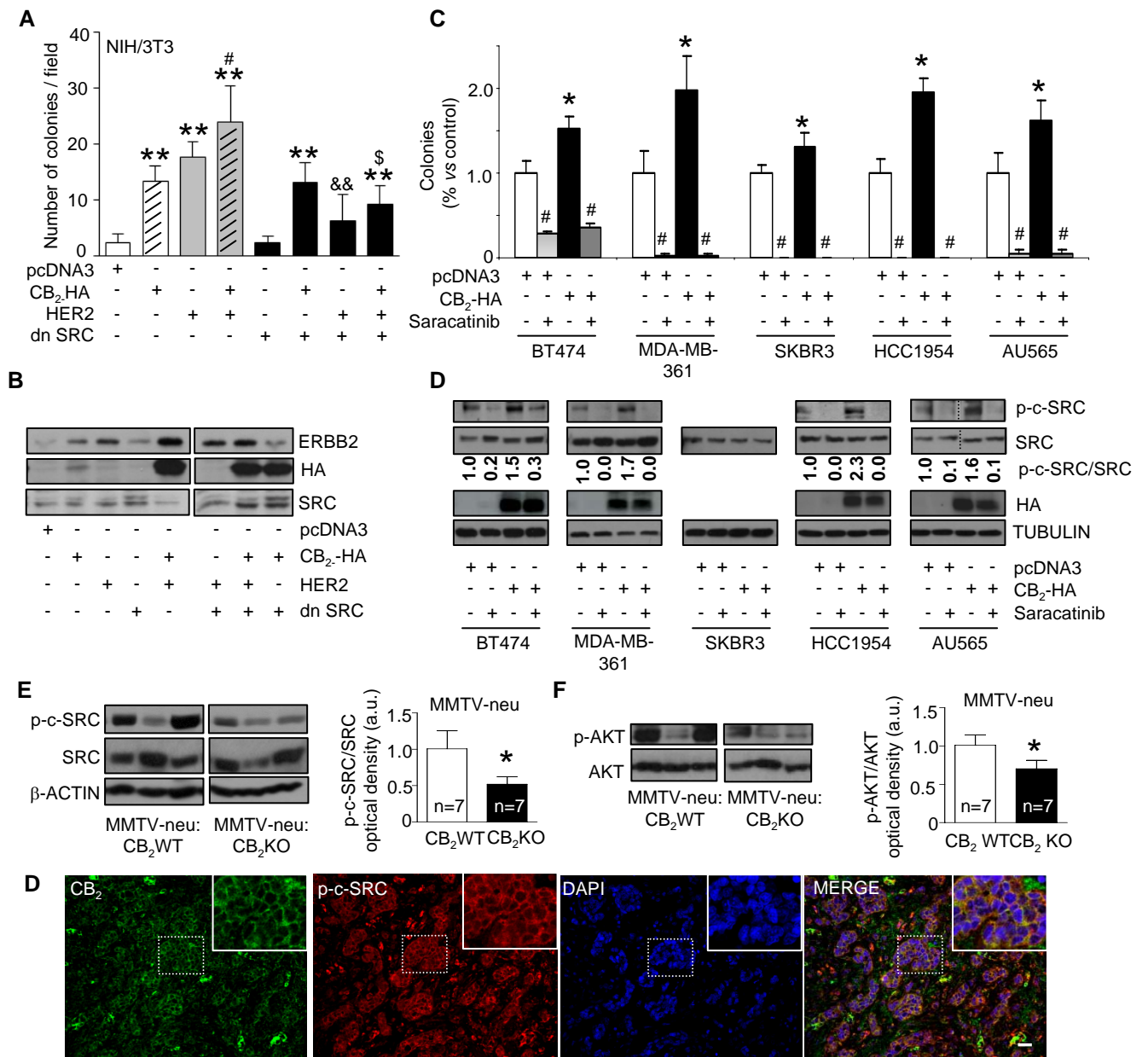
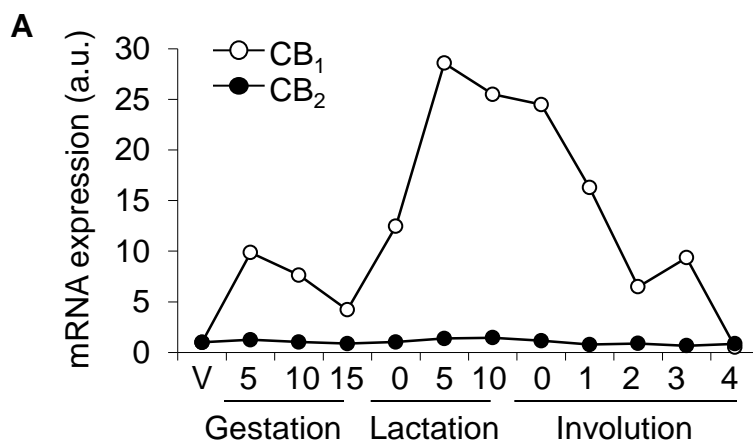


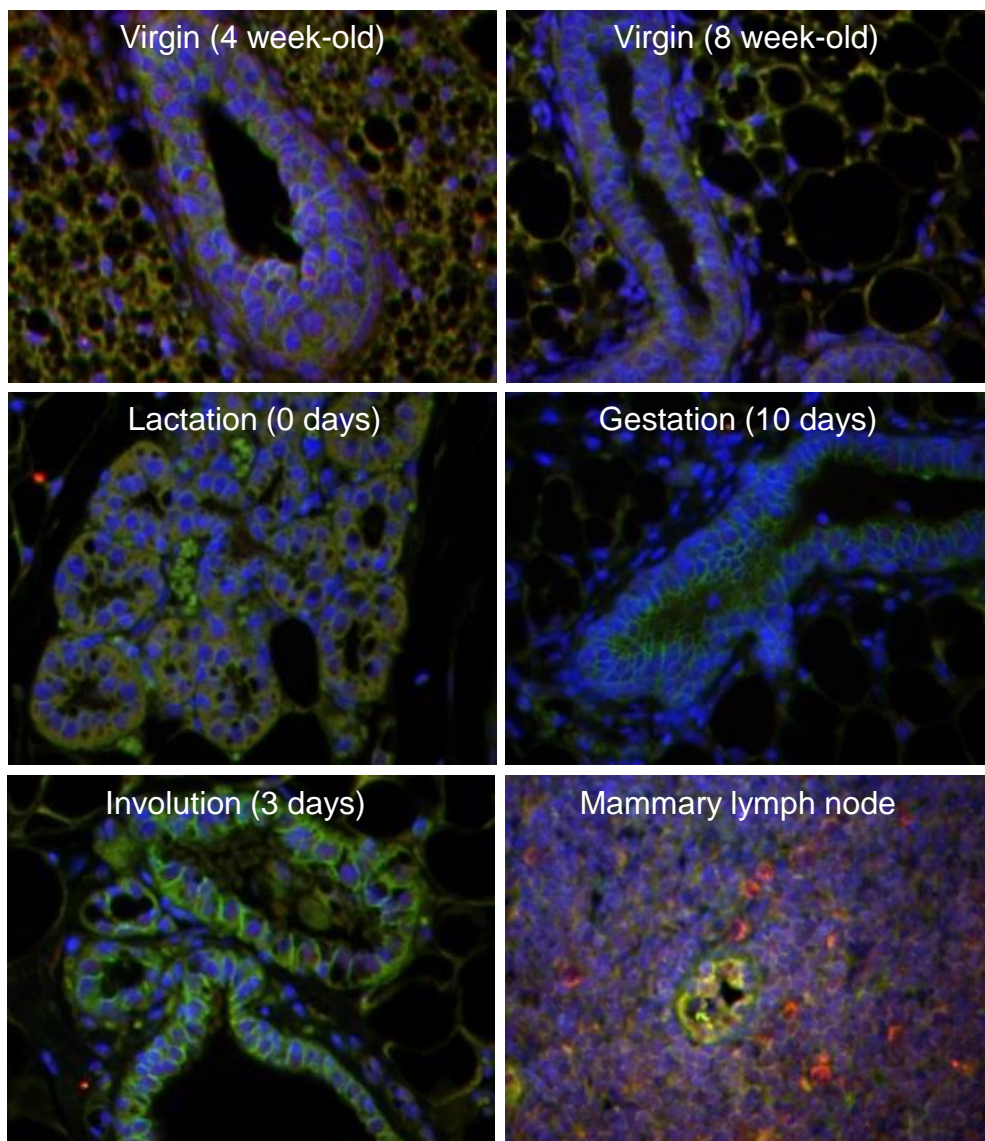
Figure 8

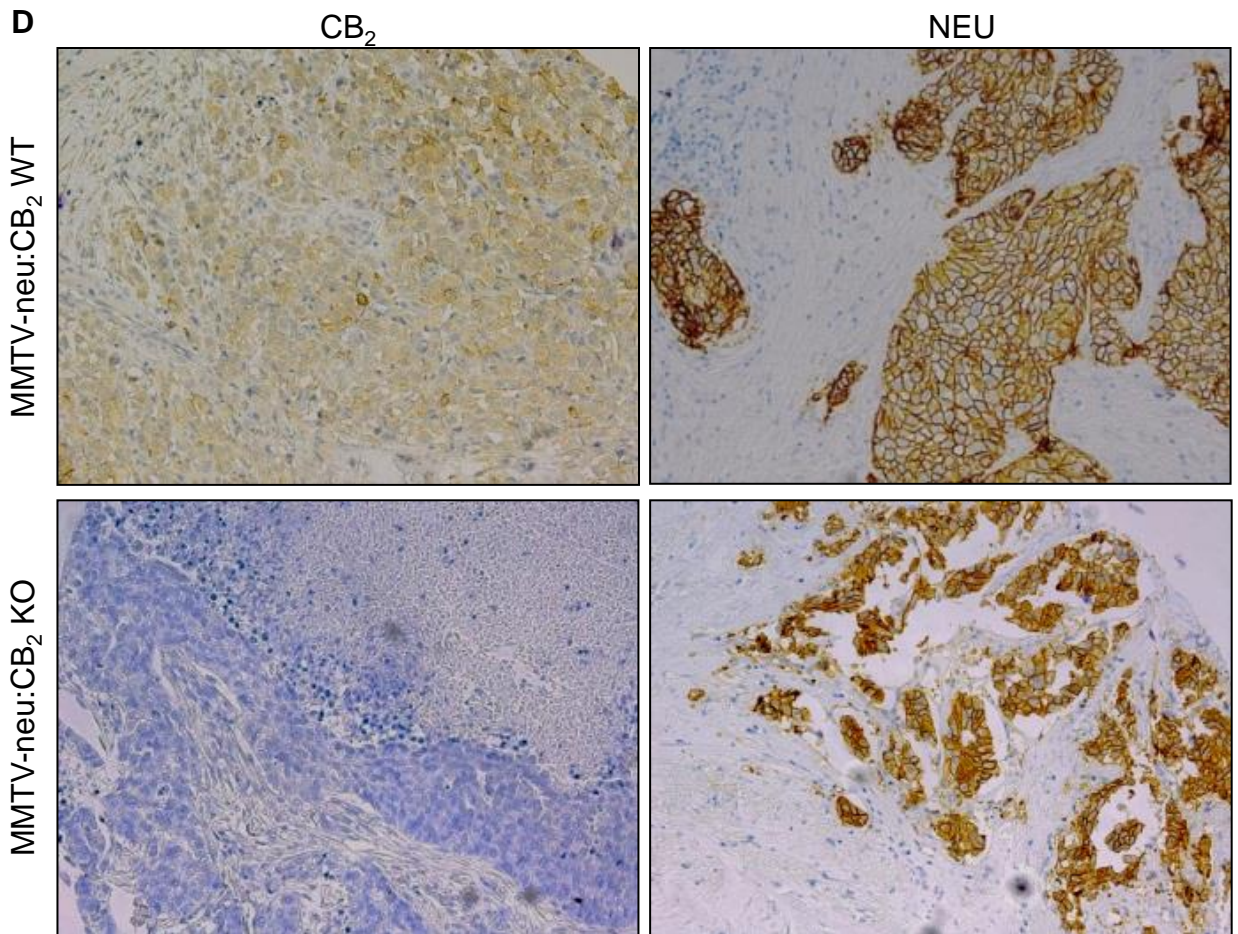
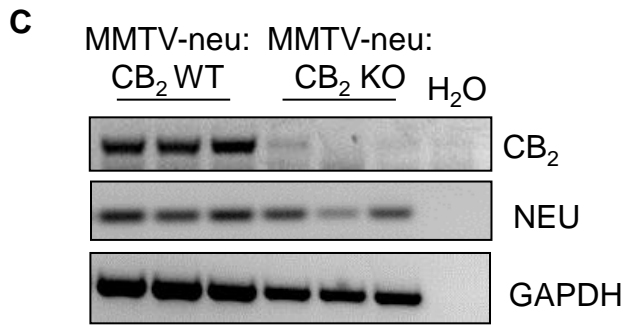


Supplementary Figure 1



B



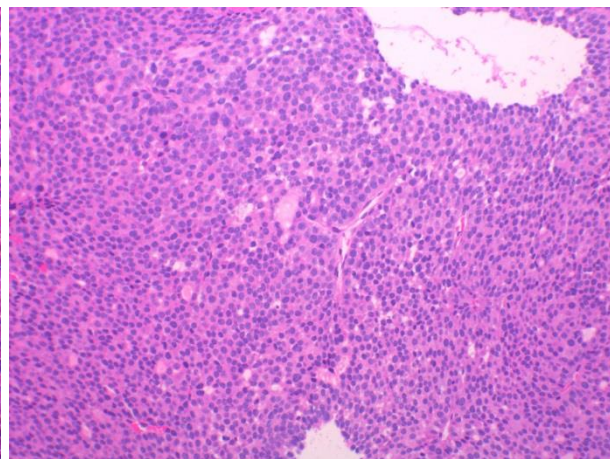
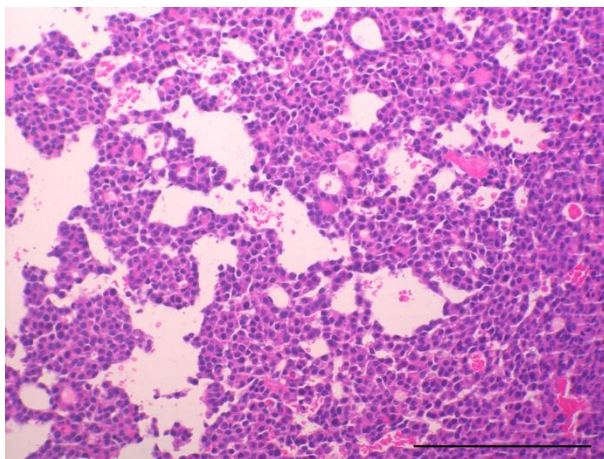


MMTV-neu:CB₂ WT

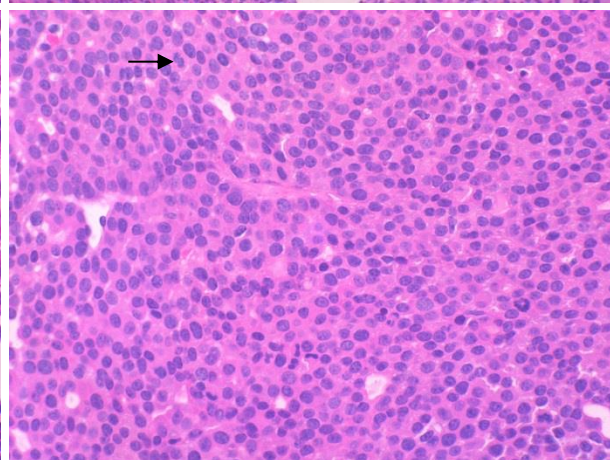
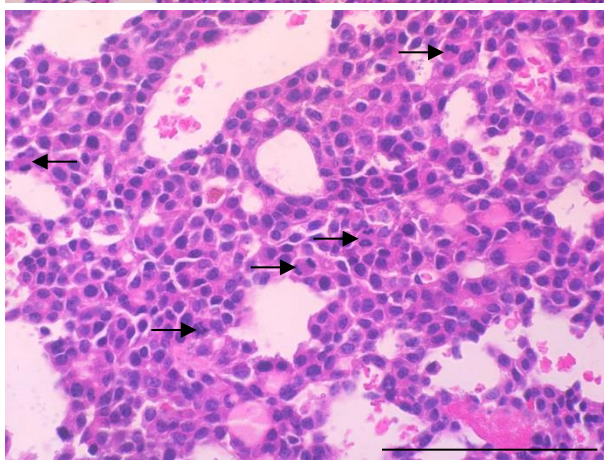
MMTV-neu:CB₂ KO

E

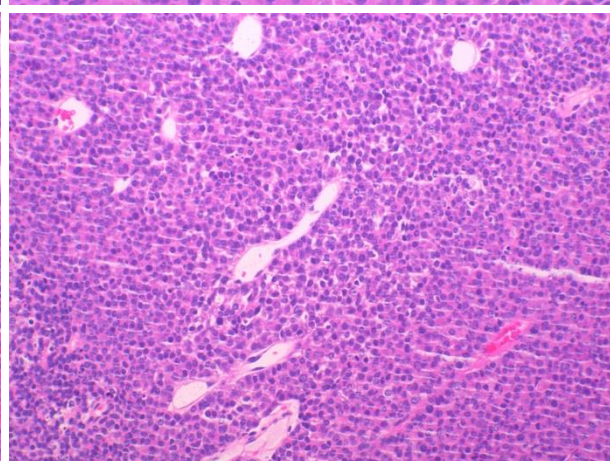
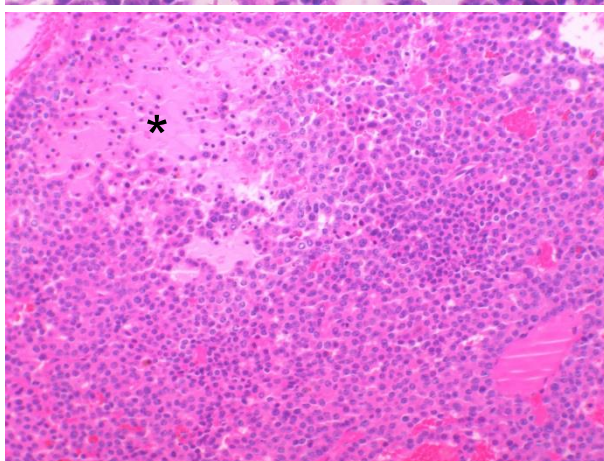
T0



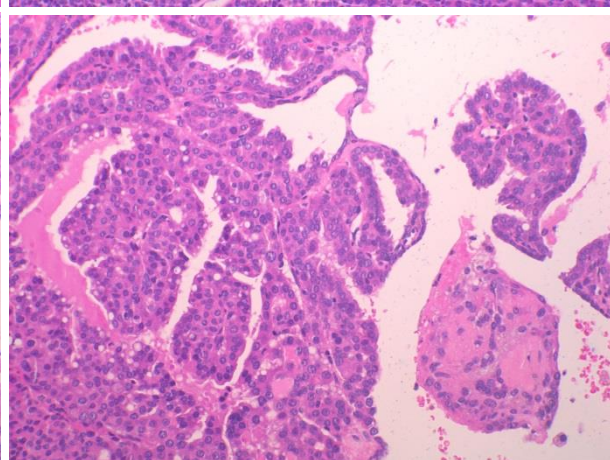
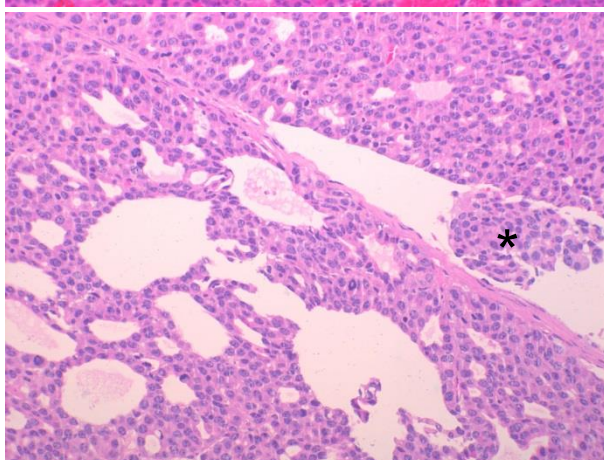
T0

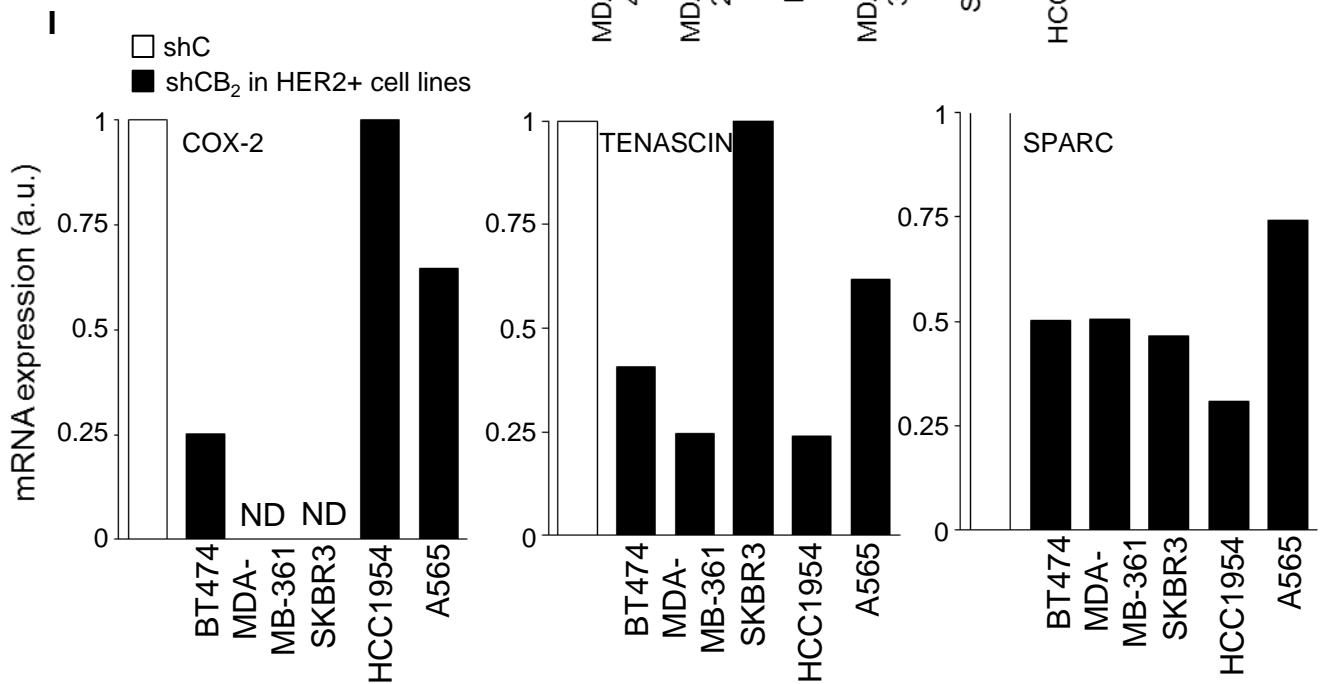
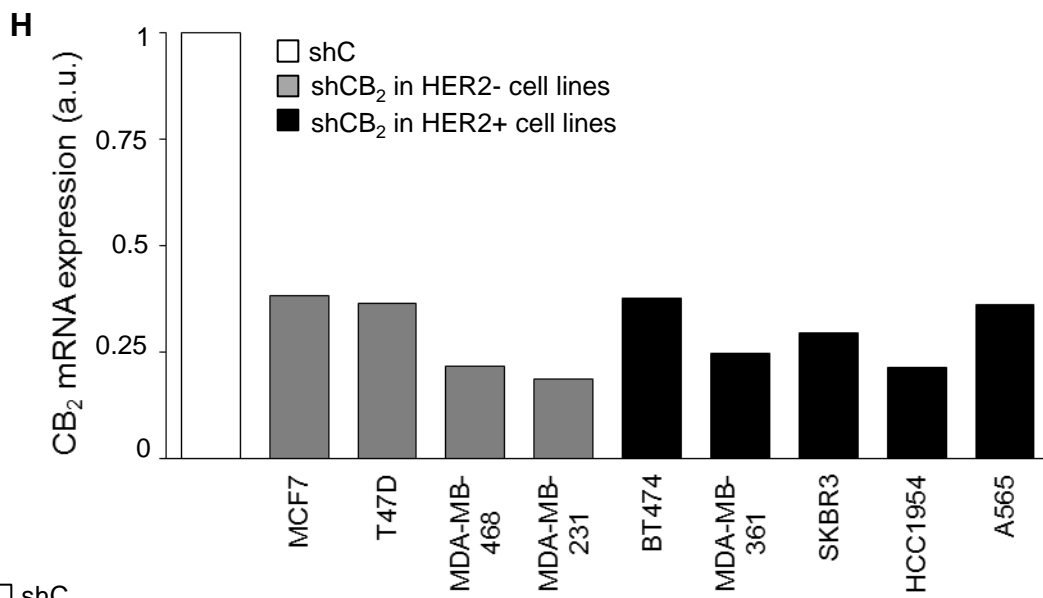
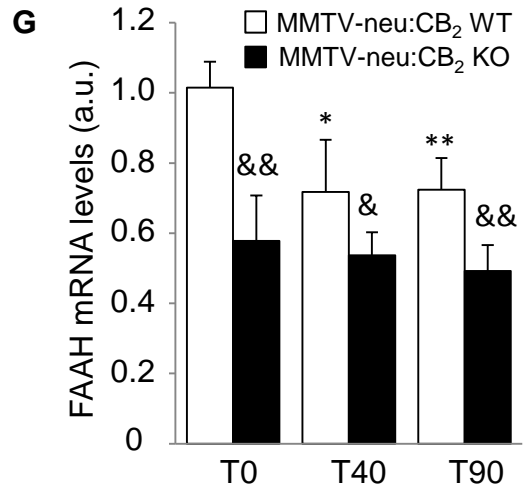
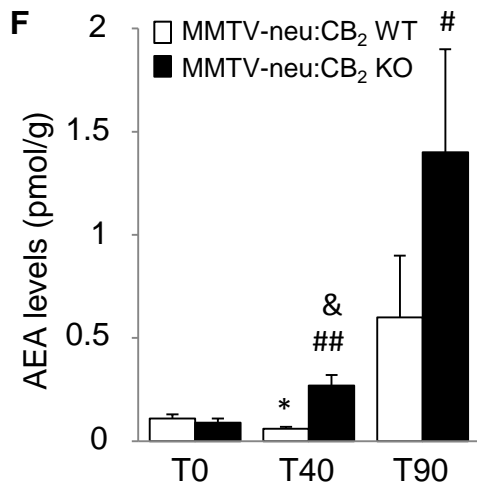


T40



T90





Supplementary Figure 1. (A-G) Mice tumour characterization. A) Analysis of CB₁ and CB₂ mRNA expression by microarray analysis in non-cancerous mammary glands of adult wild-type C57Bl/6 mice at the indicated time points of the pregnancy cycle. V, 8 week-old virgin mice. Time is expressed in days. **B)** Immunofluorescence staining of CB₂ (red) in representative tissue sections of the different stages of the adult mammary gland development. E-Cadherin (green) staining was performed for epithelial cell visualization and cell nuclei were stained in blue. A mammary lymph node is shown as a positive control of CB₂ expression. **C-D)** CB₂ and NEU mRNA [as determined by RT-PCR (**C**)] and protein expression [as determined by immunohistochemical analysis (**D**)] in representative tumour samples obtained from MMTV-neu:CB₂ WT and MMTV-neu:CB₂ KO mice. **E)** H&E staining of tumour sections obtained at tumour arousal (T0) or forty (T40) or ninety (T90) days after tumour appearance. Scale bars, 200 μm except in T0 lower pannels (100 μM). Arrows point to cells undergoing mitosis. * in WT T40 shows a necrotic area, and in WT T90 a lymphatic invasion. **F-G)**, Anandamide levels [AEA, as determined by LC-MS (**F**)] and FAAH mRNA levels [as determined by real-time quantitative PCR (**G**)] in tumour samples from the indicated animals at the indicated time points. (**H** and **I**) mRNA expression of the indicated proteins in HER2- (grey bars) and HER2+ (black bars) breast cancer cell lines upon stable transfection with a shRNA selectively targeting CB₂ (shCB₂). Results are expressed in arbitrary units vs the corresponding shC transfected cells, set at 1 (white bars). ND, non detected. *, p<0,05 and **, p<0,01 vs MMTV-neu:CB₂ WT T0; #, p<0,05 and ##, p<0,01 vs MMTV-neu:CB₂ KO T0; &, p<0,05 and &&, p<0,01 vs the corresponding WT.

Supplementary Methods

Generation of MMTV-neu:CB₂^{-/-} mice and sample collection

Generation of the congenic strain MMTV-neu:CB₂^{-/-} was accomplished by mating MMTV-neu mice (The Jackson Laboratory, Bar Harbor, Maine) with CB₂^{-/-} mice (NIH, Bethesda, Maryland). To transfer the CB₂ line (with a C57BL/6J background) to the genetic background of the tumor-prone animals (FVB/NJ), the descendants were backcrossed with MMTV-neu mice for 6 generations, using a marker-assisted selection protocol (MASP) (1). In short, the offspring of each generation was genotyped for CB₂. Heterozygous animals were genotyped for a set of 377 single nucleotide polymorphisms (SNPs) using the Mouse Low Density Linkage Panel from Illumina®. Selected breeders for the next generation were those with the highest percentage of FVB/NJ-linked SNPs. After 6 backcrosses, animals presented more than 99% FVB/NJ background. CB₂^{+/-} mice from this generation were then crossed between them to generate MMTV-neu:CB₂^{-/-} and their corresponding control littermates (MMTV-neu:CB₂^{+/+}). A total of 53 MMTV-neu:CB₂^{+/+} (10 for each time point 1 and 2, and 33 for time point 3) and 46 MMTV-neu:CB₂^{-/-} (10 for each time point 1 and 2, and 26 for time point 3) female mice were analyzed.

After animal sacrifice, mammary glands and lungs were fixed in 4% paraformaldehyde (PFA). Before PFA fixation, lungs were visually analyzed for macroscopic metastases. Microscopic metastases were determined by H&E staining of PFA-fixed paraffin-embedded sections. Tumors were divided in four portions for 1) preparation of tissue sections for immunofluorescent staining [frozen in Tissue-Tek (Sakura Finetek Europe, Zoeterwoude, The Netherlands)], 2) preparation of tissue sections for H&E staining (fixed in buffered 4% PFA), 3) protein extraction (snap frozen), and 4) RNA isolation (snap frozen), and were stored at -80°C until analysis (except PFA-fixed tumor fractions, that were kept at room temperature).

Generation of xenografts

For the generation of orthotopic tumors, 2x10⁶ viable cells were injected into the fourth right mammary fat pad of anesthetized 6 week-old SCID female mice (Harlan Interfauna Iberica, Barcelona, Spain). Tumor volume was routinely measured, and 50

days after tumor detection, animals were sacrificed and tumors were collected and processed as described above.

Generation of lung metastases

231/LM2-4 luciferase-expressing cells [a lung-seeking metastatic variant of the MDA-MB-231-HER2 cell line (2)] (5×10^5) were injected into the lateral tail vein of 6 week-old SCID female mice. Forty five days after cell injection, animals were analyzed by bioluminescence in an IVIS 2000 system (Xenogen Corp, Alameda, CA). Imaging data were processed with Living Image software (Xenogen Corp). Mice were then sacrificed and lungs were collected for metastatic nodule quantification by H&E staining.

Western blot analysis

Lysates from tumors and cell lines were subjected to SDS-PAGE, and proteins transferred onto PVDF membranes. Blots were incubated with the antibodies indicated in Supplementary Table 1. Luminograms were obtained with the Amersham Enhanced Chemiluminescence Detection Kit (GE Healthcare, Uppsala, Sweden) and densitometric analysis was performed with Quantity One software (Bio-Rad, Madrid, Spain).

RT- and real-time quantitative (Q)-PCR, and analysis of published microarray datasets

RNA was isolated with Trizol Reagent (Invitrogen, Barcelona, Spain) with the Real Star Kit (Durviz, Valencia, Spain), and cDNA was obtained with Transcriptor Reverse Transcriptase (Roche Applied Science, Barcelona, Spain). The primers used for RT- and Q-PCR are in Supplementary Table 2. For Q-PCR, probes were from the Universal Probe Library (Roche Applied Science) and multispecies 18S RNA was used as reference. For RT-PCR, GAPDH was used as reference. CB1 and CB2 mRNA expression in mouse mammary tissue was analyzed in the dataset published in (3). Human CB2 and ELK1 mRNA expression were obtained from microarray datasets published in (4), (5), (6), (7), (8), (9), (10) and (11). **The combined raw gene expression of the first 6 micro-array datasets was obtained from the “R2: microarray analysis and**

visualization platform” (<http://r2.amc.nl>), specifically from the Tumor Breast compendium -Halfwerk-947-complex-u133a.

Immunofluorescence analysis

Tissue-Tek or paraffin-embedded sections were fixed in 10% PFA and subjected to heat-induced antigen retrieval in citrate buffer before exposure to the primary antibodies indicated in Supplementary Table 1. Cell nuclei were stained with DAPI (Invitrogen). Fluorescence confocal images were acquired by using Leica TCS-SP2 software (Leica, Wetzlar, Germany). Immunofluorescence analysis of CB2 receptor was performed in mammary gland sections from wild type C57Bl/6 mice at different points of the mammary gland development as previously described (12).

Cell cultures, siRNA, shRNA, dominant negative and overexpression experiments

The following cell lines were from ATCC-LGC (Barcelona, Spain): MDA-MB-231 and MDA-MB-468 (ER-/PR- and HER2-), MCF-7 and T47D (ER+ and HER2-), and BT474, MDA-MB-361, SKBr3, HCC1954 and AU565 (HER2+) human breast adenocarcinoma cells, HEK cells and NIH/3T3 mouse embryonic fibroblasts. MDA-MB-231-HER2 cells (a MDA-MB-231 variant that stably overexpresses HER2 (13)) and 231/LM2-4 cells were kindly donated by Dr. Kerbel (University of Toronto, Canada). All cell lines (except BT474, which was cultured in RPMI) were maintained in DMEM supplemented with 10% FBS. To stably knockdown CB2, lentiviral particles containing 3 target-specific shRNA constructs were used. A scrambled shRNA construct was used as control (Santa Cruz Biotechnology, Santa Cruz, CA). Stably infected cells were selected with puromycin. For transient knock-down, a pool of double-stranded siRNA duplexes for human ELK1 (Thermo Scientific, Spain) were used. Sequences were: 5'-GCAAGGCAAUGGCCACAUC-3', 5'-CGGAAGAGCUUAAUGUGGA-3', 5'-GCCAGAAGUUCGUCUACAA-3', and 5'-GCAGCAGCCGGAACGAGUA-3'. The nontargeted control siRNA was from Applied Biosystems-Ambion (Austin, TX) and the sequence was 5'-UUCUCCGAACGUGUCACGU-3'. DharmaFECT 3 (Thermo Scientific) was used as transfection reagent. For overexpression experiments, pLNCX-cSRC K296R/Y528F [dominant negative (Millipore Iberica, Madrid, Spain)], pcDNA3-HA-hCB2 (University

of Missouri-Rolla cDNA Resource Center, Rolla, MO), pcDNA3-hERBB2 (kindly donated by Dr. Pandiella, Cancer Research Center, Salamanca, Spain), or the corresponding empty vector (pcDNA3, Invitrogen) were used. Lipofectamine 2000 (Invitrogen) was used as transfection reagent. Cell viability was determined by the MTT test (Sigma-Aldrich, Spain) according to manufacturer's instructions.

Chromatin immunoprecipitation (ChIP) assays

Cells were processed as recommended by the manufacturer (EZ-ChIP, Millipore) and immunoprecipitation was performed with an anti-ELK1 antibody (Supplementary Table 1) or a non-specific rabbit IgG as control. ELK1-bound DNA was determined by RT-PCR analysis. Primers for the amplification of ELK1-binding DNA sequences in the CB2 promoter region (14) were: Forward: 5'-TGGTAACAGGCACGGAAGGC-3'; Reverse: 5'-TGAGTGCCACCCCAAGCCAG-3'.

Co-immunoprecipitation experiments

HEK-293T cells were transiently transfected with expression vectors pcDNA3-HA-hCB2, pcDNA3-hERBB2 and pcDNA3 empty vector, using Lipofectamine Plus as transfection agent. Cells were lysed in IP buffer and proteins were immunoprecipitated using anti-HA or anti-ERBB2 antibodies (Supplementary Table 1) coupled to protein G-Sepharose.

In situ proximity ligation assays

Heteromers were detected using the Duolink II in situ PLA detection Kit (OLink Bioscience, Uppsala, Sweden). Cells were incubated with a mixture of equal amounts of anti-HER2 antibody (Supplementary Table 1) directly coupled to a DNA plus chain, and anti-CB2 antibody (Supplementary Table 1) directly coupled to a DNA minus chain, obtained following the instructions of the supplier. Amplification was done with the Duolink II Detection Reagents Red Kit. The samples were observed in a Leica SP2 confocal microscope. Images were processed with Image J software.

Anchorage-independent growth

Cells were suspended in DMEM supplemented with 10% FBS and 0.35% agar, layered on top of a solid 0.5% agar base in 6-well plates, and incubated at 37°C and 5% CO₂ for 45 days. The resulting colonies were morphologically assessed and quantified after staining with crystal violet.

Cell invasion

Cells were suspended in DMEM and loaded onto the upper compartment of BD BioCoat Matrigel Invasion Chambers (BD Biosciences, Bedford, MA). FBS (10%) was used as chemoattractant in the lower compartment. Cell invasion was quantified by staining migrated cell nuclei with DAPI.

Quantification of anandamide levels

Tissue samples were weighted and homogenized in chloroform:methanol:Tris HCl 50 mM (pH =7.5) [2:1:1 (v:v:v)]. d8-AEA (Cayman Chemical) was added as internal standard. The organic and aqueous layers were separated by centrifugation and the organic layer transferred to a clean vial and dried under a stream of argon. The resulting fraction was reconstituted in acetonitrile and analyzed by high-pressure liquid chromatography coupled to mass spectrometry (LC-MS). LC-MS analysis was performed using an Agilent 1200LC-MSD VL instrument. LC separation was achieved with a Zorbax Eclipse Plus C18 column (5 µm, 4.6 mm x 50 mm) together with a guard column (5 µm, 4.6 mm x 12.5 mm). The gradient elution mobile phases consisted of A (95:5 water:acetonitrile) and B (95:5 acetonitrile:water), with 0.1% formic acid as the solvent modifier. The gradient (flow rate of 0.5 mL/min) started at 0% B (for 5 min), increased linearly to 100% B over the course of 45 min, and decreased to 0% B for 10 minutes before equilibrating for 5 min with an isocratic gradient of 0% B. MS analysis was performed with an electrospray ionization source. LC-MS measurements were made by selected ion monitoring in positive mode. Fractions were quantified by measuring the area under the peak and normalized using d8-AEA as internal standard and absolute AEA levels were estimated by comparison with the respective deuterated standard.

Phosphoarray analysis

A phospho-kinase protein array (R&D Systems, Abingdon, UK) was used for the simultaneous analysis of 43 different phosphorylation sites by a Western blot-based technique. Cell lysates were incubated with the nitrocellulose membranes provided by the phospho-array. The array was washed to remove unbound proteins and incubated with biotinylated detection antibodies. Membranes were then incubated with streptavidin-HRP and chemoluminescence reagents. The densitometric analysis was performed with Quantity One software.

Gene promoter activity assays

A DNA fragment from the immediate upstream region of the CB2 receptor gene CNR2 (-614 to +243) was amplified by PCR using human genomic DNA as template and the following primers: Forward: 5'-CCCGGGTATACTCCCAAGCAGAAAAG-3'; Reverse: 5'-CTCGAGATACAGGTGTTGGGGAATGA-3'. The 0.85-kb PCR product was cloned using the StrataClone PCR Cloning Kit (Agilent Technologies España, Madrid, Spain) and sequenced with an ABI 3730xl sequencer using T7 reverse and T3 forward primers. Then, it was subcloned into the pGL3 luciferase reporting vector (Promega, Madison, WI) using XmaI (Thermo Scientific). To generate the pGL3-CB2 promoter plasmids containing point mutations in the predicted ELK1-binding sites, QuikChange Site-Directed Mutagenesis Kit (Stratagene, La Jolla, CA) was used with the primers indicated in Supplementary Table 2. HEK293T cells were transiently transfected with the following plasmids: pGL3-hCB2 or pGL3-hCB2 mutated plasmids in combination with pCMV5-ELK1-HA plasmid (kindly provided by Dr. Sharrocks, University of Manchester, UK); a constitutively active ELK1 construct (Ser383Asp; Ser389Asp; generated with a QuikChange Site-Directed Mutagenesis Kit; Stratagene); or an empty vector. Transcriptional promoter-driven luciferase activity was analyzed with the Dual-Luciferase Reporter Promega Assay System (Promega) in a Lumat LB9507 luminometer. Renilla-derived luciferase activity was used as internal transfection control.

Statistical analysis

The Pearson's chi-squared test was used for statistical analysis of the human samples included in the TMAs. Kaplan-Meier survival curves were statistically compared by the Logrank test. ANOVA with a post-hoc analysis by the Student–Newman–Keuls' test was routinely used for the rest of the analyses. Unless otherwise stated, data are expressed as mean±s.e.m. All statistical tests were two-sided, unless otherwise specified.

References

1. Wong GT. Speed congenics: applications for transgenic and knock-out mouse strains. *Neuropeptides*. 2002;36(2-3):230-6.
2. Munoz R, Man S, Shaked Y, et al. Highly efficacious nontoxic preclinical treatment for advanced metastatic breast cancer using combination oral UFT-cyclophosphamide metronomic chemotherapy. *Cancer Res*. 2006;66(7):3386-91.
3. Clarkson RW, Watson CJ. Microarray analysis of the involution switch. *J Mammary Gland Biol Neoplasia*. 2003;8(3):309-19.
4. Chin K, DeVries S, Fridlyand J, et al. Genomic and transcriptional aberrations linked to breast cancer pathophysiologies. *Cancer Cell*. 2006;10(6):529-41.
5. Bild AH, Yao G, Chang JT, et al. Oncogenic pathway signatures in human cancers as a guide to targeted therapies. *Nature*. 2006;439(7074):353-7.
6. Loi S, Haibe-Kains B, Desmedt C, et al. Definition of clinically distinct molecular subtypes in estrogen receptor-positive breast carcinomas through genomic grade. *J Clin Oncol*. 2007;25(10):1239-46.
7. Miller LD, Smeds J, George J, et al. An expression signature for p53 status in human breast cancer predicts mutation status, transcriptional effects, and patient survival. *Proc Natl Acad Sci U S A*. 2005;102(38):13550-5.
8. Pawitan Y, Bjohle J, Amler L, et al. Gene expression profiling spares early breast cancer patients from adjuvant therapy: derived and validated in two population-based cohorts. *Breast Cancer Res*. 2005;7(6):R953-64.
9. Desmedt C, Piette F, Loi S, et al. Strong time dependence of the 76-gene prognostic signature for node-negative breast cancer patients in the TRANSBIG multicenter independent validation series. *Clin Cancer Res*. 2007;13(11):3207-14.

10. Hatzis C, Pusztai L, Valero V, et al. A genomic predictor of response and survival following taxane-anthracycline chemotherapy for invasive breast cancer. *JAMA*. 2011;305(18):1873-81.
11. Minn AJ, Gupta GP, Siegel PM, et al. Genes that mediate breast cancer metastasis to lung. *Nature*. 2005;436(7050):518-24.
12. Caffarel MM, Zaragoza R, Pensa S, et al. Constitutive activation of JAK2 in mammary epithelium elevates Stat5 signalling, promotes alveologenesis and resistance to cell death, and contributes to tumourigenesis. *Cell Death Differ*. 2011;19(3):511-22.
13. du Manoir JM, Francia G, Man S, et al. Strategies for delaying or treating in vivo acquired resistance to trastuzumab in human breast cancer xenografts. *Clin Cancer Res*. 2006;12(3 Pt 1):904-16.
14. Sherwood TA, Nong L, Agudelo M, et al. Identification of transcription start sites and preferential expression of select CB2 transcripts in mouse and human B lymphocytes. *J Neuroimmune Pharmacol*. 2009;4(4):476-88.